

DRAN: A Distribution and Relation Adaptive Network for Spatio-temporal Forecasting

Xiaobei Zou, Luolin Xiong, Kexuan Zhang, Cesare Alippi, *Fellow, IEEE*, Yang Tang, *Fellow, IEEE*

Abstract—Accurate predictions of spatio-temporal systems are crucial for tasks such as system management, control, and crisis prevention. However, the inherent time variance of many spatio-temporal systems poses challenges to achieving accurate predictions whenever stationarity is not granted. In order to address non-stationarity, we propose a Distribution and Relation Adaptive Network (DRAN) capable of dynamically adapting to relation and distribution changes over time. While temporal normalization and de-normalization are frequently used techniques to adapt to distribution shifts, this operation is not suitable for the spatio-temporal context as temporal normalization scales the time series of nodes and possibly disrupts the spatial relations among nodes. In order to address this problem, a Spatial Factor Learner (SFL) module is developed that enables the normalization and de-normalization process in spatio-temporal systems. To adapt to dynamic changes in spatial relationships among sensors, we propose a Dynamic-Static Fusion Learner (DSFL) module that effectively integrates features learned from both dynamic and static relations through an adaptive fusion ratio mechanism. Furthermore, we introduce a Stochastic Learner to capture the noisy components of spatio-temporal representations. Our approach outperforms state-of-the-art methods on weather prediction and traffic flow forecasting tasks. Experimental results show that our SFL efficiently preserves spatial relationships across various temporal normalization operations. Visualizations of the learned dynamic and static relations demonstrate that DSFL can capture both local and distant relationships between nodes.

Index Terms—Spatio-temporal forecasting, graph neural network, distribution adaptation, adaptive network.

I. INTRODUCTION

Spatio-temporal systems, characterized by intricate spatial interactions among sensors (nodes) and rich temporal dynamics, are prevalent in various fields e.g., physics [1], meteorology [2]–[4], power grids [5]–[7] and transportation [8], [9]. Such systems often entail a large number of nodes, with interactions among nodes varying over time [10], [11]. The complexity of these systems and the time variance makes it challenging to efficiently manage future system developments and decision-making, hence requiring more accurate spatio-temporal prediction [12].

In spatio-temporal forecasting, historical time series data associated with nodes are used to predict future observations

This work was supported by the National Natural Science Foundation of China (62293502, 62293504, 62173147). (Corresponding author: Yang Tang.)

Xiaobei Zou, Luolin Xiong, Kexuan Zhang and Yang Tang are with the Key Laboratory of Smart Manufacturing in Energy Chemical Process, Ministry of Education, East China University of Science and Technology, Shanghai 200237, China (e-mail: xbeizou@gmail.com; xiongluolin@gmail.com; kexuanhang123@gmail.com; yangtang@ecust.edu.cn).

Cesare Alippi is with the Faculty of Informatics, Università della Svizzera italiana, 69000 Lugano, Switzerland, and also with the Department of Electronics, Information and Bioengineering, Politecnico di Milano, 20133 Milan, Italy (e-mail: alippi@elet.polimi.it).

[13], [14]. Although numerous effective methods, particularly those based on deep learning, have been developed [15]–[17], predictions remains challenging due to the time variance of the environment-system interaction. This time variance can manifest in several ways, e.g., distribution shifts [18], [19], changes in spatial relationships among nodes [20], and changes in the nature of noise [21].

Normalization and de-normalization mechanisms are commonly employed to address distribution shifts in time series forecasting, particularly in scenarios that show temporal variation without strong spatial interactions [22]–[25]. Normalization is applied to the input data to align its distribution with that of the training set, while de-normalization maps the processed results back to the original temporal distribution. However, above methods, which apply normalization and de-normalization on instance [22] or temporal dimensions [25], may not be well-suited for processing spatio-temporal data using graph neural networks that rely on relational inductive bias. In fact, temporal normalization scales the time series of nodes using different scaling factors as the temporal content evolves with time variance, hence causing erroneous scaled spatial messages propagating between nodes. Moreover, instance-level normalization uses the mean and standard deviation of all nodes over the input time span, addressing only coarse spatial and temporal distribution shifts, which is inadequate for adapting to the complex distributions in spatio-temporal contexts. Therefore, it is necessary to develop approaches that achieve temporal normalization while preserving spatial patterns in spatio-temporal forecasting tasks.

Various methods have been proposed to capture time-varying spatial relationships, including learning inherent static spatial structures from data [26]–[28], generating dynamic dependencies based on input windows [29], [30], and jointly modeling static and dynamic components through weighted fusion [31] or loss-constrained fusion ratios [32]. However, these approaches often overlook the dynamic interplay between static and dynamic spatial components, relying on fixed fusion schemes. This can lead to suboptimal spatio-temporal representations, especially in scenarios where the relative importance of static and dynamic features varies over time. Therefore, there is a pressing need for methods capable of adapting to both static and dynamic relations.

In addition, spatio-temporal systems are inherently affected by various sources of uncertainty, including data inaccuracies, sensor noise, and sudden stochastic events that might change with time. Given that these uncertainties impact prediction performance, various efforts have been made to quantify them. Some studies perform interval prediction to provide confidence

regions for the forecasting horizon [33], [34]. Liang *et al.* [35] utilize latent variables to capture the uncertainties in air quality data, enhancing the accuracy of predictions.

In this paper, we propose a Distribution and Relation Adaptive Network (DRAN) that dynamically adapts to temporal variations and assesses uncertain components influenced by noise to achieve more comprehensive representation learning in spatio-temporal systems. More specifically, we develop a Spatial Factor Learner (SFL) that incorporates temporal normalization and de-normalization stages to mitigate the impact of distribution shifts while preserving spatial dependencies. To better accommodate spatio-temporal relations, we introduce a Dynamic-Static Fusion Learner (DSFL) module that merges features learned from sample-specific dynamic and static relations using an adaptive fusion ratio mechanism. Additionally, we propose a Stochastic Learner based on a Variational Autoencoder (VAE) to estimate uncertainty. Experimental validations on weather and traffic systems demonstrate that our model outperforms state-of-the-art methods. **The novelty of our method can be summarized as follows:**

- We introduce an SFL module that enables a normalization and de-normalization **mechanisms** for distribution adaptation in a spatio-temporal context. The SFL module reverses temporal normalization while ensuring that spatial distributions closely match those of the forecasting horizons.
- Different from previous spatio-temporal relations adaptive methods which fuse dynamic and static features with a fixed ratio [31], [32], [36], [37], we propose a DSFL module to adaptively combine features from both dynamic and static relations with a gating mechanism, **accommodating the changing relations**.
- We propose a framework to **learn both deterministic and stochastic spatio-temporal representations**, where a VAE-based Stochastic Learner is introduced to capture the noisy components of the representations.

The paper is organized as follows. Section II introduces the **state of the art**. Section III details our network architecture and the overall workflow. Section IV describes the experimental setups, including dataset descriptions, network configurations, training procedures, and baseline comparisons. Section V presents the numerical results for traffic flow and weather predictions, accompanied by an ablation study and visualizations of module impacts. **The discussion is provided in Section VI**, and the conclusion in Section VII.

II. RELATED WORKS

A. Spatio-temporal forecasting

Spatio-temporal forecasting is a longstanding and important research task. Early approaches primarily employed statistical models such as Historical Average (HA) and ARIMA [38]–[40], which offer interpretability but struggle to capture complex spatio-temporal dependencies. With the advent of deep learning, various modules are developed to model temporal and spatial dependencies more effectively. For temporal modeling, recurrent and convolutional neural networks [41]–[43] show effectiveness in short-term forecasting, while

transformer-based architectures and state space models [44] demonstrate strong performance in both short- and long-term forecasting. Recurrent networks update historical information through hidden states, whereas transformer-based methods use attention mechanisms to capture dependencies from time-point [45], patch [46], and frequency-domain perspectives [47], [48]. To model spatial dependencies, both explicit and implicit methods have been proposed. Explicit methods typically utilize graph-based structures to represent node-link relationships and facilitate message propagation [28]. In contrast, implicit methods encode spatial dependencies within network parameters or attention mechanisms [49]–[51]. Despite promising performance, many existing methods still struggle with capturing evolving spatial structures and often lack interpretability. To address these issues, decomposition-based approaches emerge as a promising direction. These methods decompose temporal signals into trend and seasonal components [52], [53], extract multi-frequency patterns [54], and learn multi-scale spatial relationships [55], [56]. In this work, we propose a framework that decomposes spatial relations into dynamic and static components while learning both deterministic and stochastic features.

B. Static and dynamic Relation Learning

Spatio-temporal forecasting methods are designed to capture both the static and dynamic relations existing among nodes. Static relations are typically learned from training datasets using trainable embeddings and adjacency matrices to depict inter-node relationships [16], [57], [58]. Conversely, other studies [59], [60] construct dynamic networks by generating sample-specific relations, which can be derived either directly from each input time series based on node similarity [56], [61] or through the use of meta-learners that generate dynamic parameters [62], [63]. Additionally, some methods refine the original relationships with input features [20], [64]. Furthermore, certain approaches simultaneously learn static and dynamic relations and integrate the gathered information. For instance, Fang *et al.* [32] decompose spatial relations into static and dynamic components, using a min-max learning paradigm with hyperparameters to simultaneously learn both aspects. Similarly, Li *et al.* [31] employ two parallel Graph Convolutional Networks (GCNs) to learn static and dynamic information, which is then fused using a weighted sum. These methods typically fuse the static and dynamic features at a fixed ratio. **In this work, we focus on the adaptive fusion of dynamic and static spatial relations.**

C. Adaptation to Distribution Shifts

Normalization methods utilize statistic properties to normalize and de-normalize time series, adapting to distribution shifts in systems. Commonly, these methods utilize the mean and variance of input time series for data normalization. RevIN [22] employs a learnable affine transformation to align the means and standard deviations of inputs with those of outputs, facilitating distribution removal and reconstruction. Non-stationary Transformer [23] argues that existing stationary methods remove excessive information from time series, which

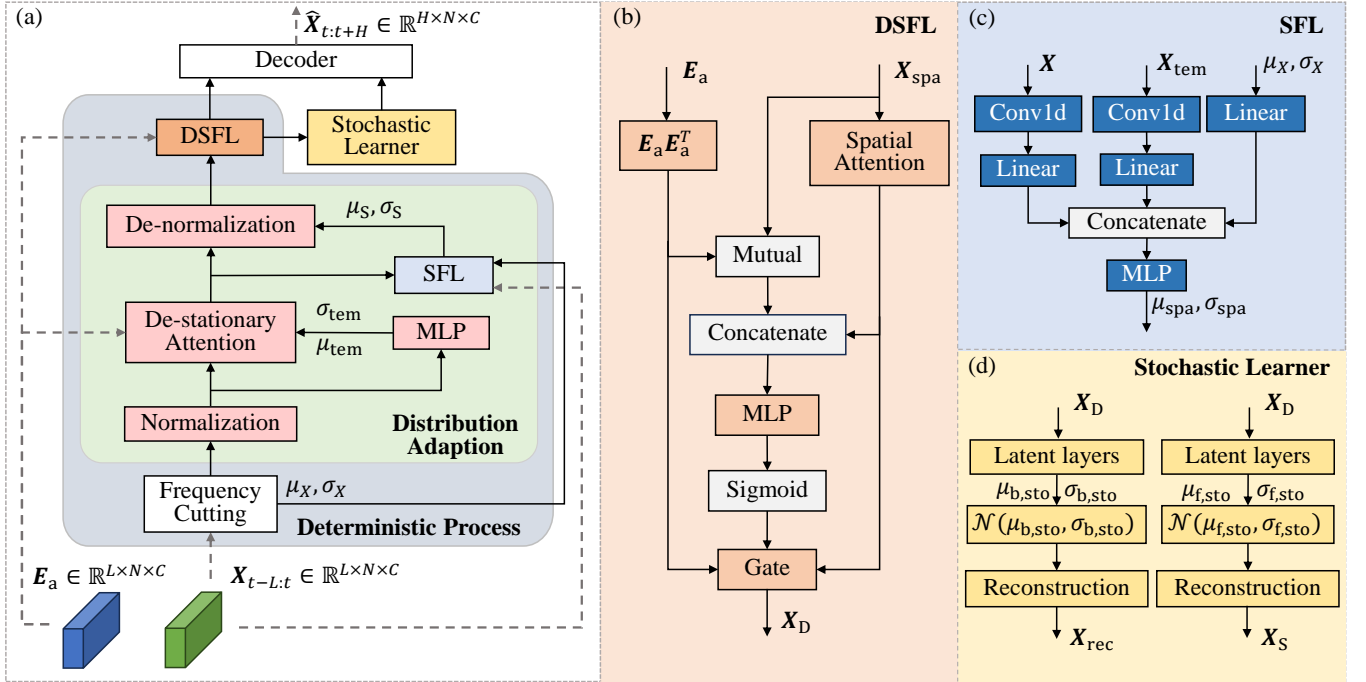


Fig. 1. The architecture of DRAN. (a) provides an overview of DRAN, which learns both the deterministic (grey) and stochastic (yellow) components of the spatio-temporal representations. In learning the deterministic components, a normalization and de-normalization process (green) is conducted using the Spatial Factor Learner (SFL) module to achieve distribution adaptation. The Dynamic-Static Fusion Learner (DSFL) module (orange) learns spatial dependencies from both dynamic and static perspectives and fuses them using an adaptive ratio. (b), (c), and (d) offer detailed views of the structures of the DSFL, SFL, and Stochastic Learner, respectively.

hampers the model's ability to learn temporal dependencies. To address this, it introduces De-stationary Attention modules that aim to balance this trade-off. Deep Adaptive Input Normalization (DAIN) [19] implements linear and gated layers to learn adaptive scaling and shifting factors for normalization. ST-Norm [65] proposes temporal and spatial normalization modules, which separately refines the high-frequency component and the local component of features. Additionally, U-Mixer [66] employs covariance analysis to correct stationarity for each feature. EAST-Net [67] generates sequence-specific network parameters to adapt dynamically to events.

III. METHODOLOGY

A. Problem Definition

The observed variables of node i at time step t can be referred to as a C -dimensional vector $\mathbf{X}_{t,i} \in \mathbb{R}^C$. Each observation at time step t is the result of a stochastic process, drawn from a conditioned distribution $\mathbf{X}_{t,i} \sim p_{t,i}(\mathbf{X}_{t,i} | \mathbf{X}_{t-1}, \mathbf{X}_{t-2}, \dots, \mathbf{X}_{t-k}, \dots)$, where $\mathbf{X}_{t-k} \in \mathbb{R}^{N \times C}$ denotes the observations from N nodes at time step $t-k$ in the spatio-temporal framework. The probability distribution $p_{t,i}$ varies over time and differs across nodes, indicating that distribution shifts occur when observations across different time periods exhibit distinct distributions, i.e.,

$$D(p_{t_k,i}, p_{t_l,i}) > \delta,$$

where $\delta > 0$ is a small threshold, $D(\cdot, \cdot)$ is a distance function that estimates the discrepancy between distributions, and t_k

and t_l refer to two different time steps. In this work, we utilize Gaussian kernel density estimation [68] for distribution estimation and use KL divergence as a distance function.

Algorithm 1 DRAN Framework

Require: Spatio-temporal dataset D_s , hyperparameter α , lookback length L , horizon length H , max epoch
Require: model parameters θ of DRAN

- 1: Initialize model parameters θ and node embedding E_a
- 2: **for** epoch = 1 to max epoch **do**
- 3: **for** each batch $\mathbf{X}_{t-L:t}, \mathbf{X}_{t:t+H} \in D_s$ **do**
- 4: Compute μ_X, σ_X
- 5: Obtain X_{Norm} via Eq (1)
- 6: $X_{tem} \leftarrow \text{DestationaryAtt}(X_{Norm}, \mu_X, \sigma_X)$ via Eq (2-4)
- 7: $\mu_{spa}, \sigma_{spa} \leftarrow \text{SFL}(X, X_{tem}, \mu_X, \sigma_X)$
- 8: Rescale according to Eq (5) and obtain X_{spa}
- 9: $X_D \leftarrow \text{DSFL}(X_{spa}, E_a)$ via Eq (6-11)
- 10: $X_S, X_{rec} \leftarrow \text{StochasticLearner}(X_D)$ via Eq (12-15)
- 11: Compute \mathcal{L} via Eq (17) and optimize θ
- 12: **end for**
- 13: **end for**
- 14: **return** model parameters θ

The goal of the spatio-temporal forecasting task is to develop a model F that uses the historical observations of length L of nodes $\mathbf{X}_{t-L:t-1} \in \mathbb{R}^{L \times N \times C}$ to predict the future H -step observations of nodes $\mathbf{X}_{t:t+H} \in \mathbb{R}^{H \times N \times C}$, where $\mathbf{X}_{t-L:t} \in \mathbb{R}^{L \times N \times C}$ refers to time series of observed variables of all the nodes $(\mathbf{X}_{t-L}, \mathbf{X}_{t-L+1}, \dots, \mathbf{X}_{t-1})$. Due to the time variance

in spatio-temporal data generation, learning a model F that effectively handles shifting distributions is challenging. The overall workflow of DRAN and the structure of its modules are depicted in Fig. 1 and detailed in Algorithm 1.

B. Distribution Adaptation

The distribution of historical time series often diverges from that of future time series due to time variance. Fig. 2 (a) demonstrates the effectiveness of temporal normalization, which aligns the historical distribution more closely with the future distribution. This alignment facilitates easier learning of the projection from the input to the forecasting horizon. Consequently, temporal normalization is both an effective and necessary operation for spatio-temporal forecasting. While

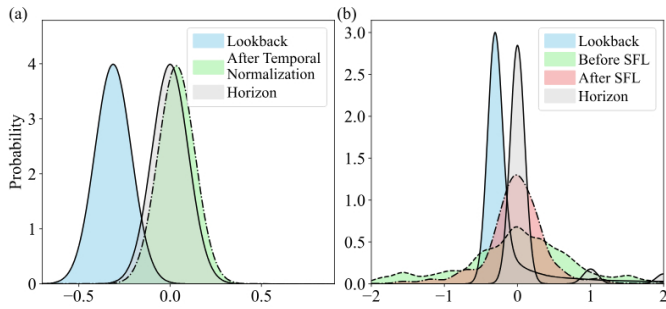


Fig. 2. Temporal and spatial distribution changes. We use the probability density function for distribution estimation and visualization. The probability density function is fitted using Gaussian Kernel Density, where the probability density at point ξ is given by $\hat{f}(\xi) = 1/mh \sum_{i=1}^m 1/2\pi e^{-(\xi-\xi_i)^2/2h^2}$ for random variables $\{\xi_1, \dots, \xi_m\}$, where h represents the parameter that controls the smoothness of the distribution and is set to 0.1 in this work. Panel (a) illustrates the temporal distribution shifts of the NYC Bike2 dataset and demonstrates the effectiveness of temporal normalization. Panel (b) displays the spatial distribution changes in the forecasting networks. "Lookback" and "Horizon" refer to the distribution of historical and future time series, respectively. Arrows of different colors represent the transformation to the horizon distributions.

previous works [23], [25] have addressed distribution shifts in multivariate time series forecasting, these methods are not suitable for time series with spatial relations. Direct application of these stationary strategies to spatio-temporal forecasting results in degraded performance. As shown in Fig. 2 (b), the direct application of normalization (colored in green) leads to spatial distributions deviating significantly from the spatial distribution of horizon windows. This is because they perform normalization within the time series of each node, leading to inconsistent scaling among nodes that are spatially interconnected. Therefore, we develop a framework that learns the temporal distribution shift on each node and preserves the spatial relations of nodes, thus maintaining the efficiency of spatial layers.

To learn the deterministic part of the inputs, the input time series is firstly filtered by removing high-frequency noise. We then normalize the input time series of each node using the temporal mean $\mu_X \in \mathbb{R}^{1 \times N \times C}$ and standard deviation $\sigma_X \in \mathbb{R}^{1 \times N \times C}$ calculated for each input window.

$$X_{\text{Norm}} = (X - \mu_X) / \sigma_X, \quad (1)$$

where X_{Norm} represents the normalized time series. To preserve essential temporal information, we incorporate temporal dependency learning through the de-stationary attention mechanism from the Non-stationary Transformer [23]. This mechanism utilizes de-stationary factors μ_{tem} and σ_{tem} , which are learned from a multilayer perceptron (MLP).

$$\log \sigma_{\text{tem}} = \text{MLP}(\sigma_X, X_{\text{Norm}}), \quad (2)$$

$$\mu_{\text{tem}} = \text{MLP}(\mu_X, X_{\text{Norm}}), \quad (3)$$

$$X_{\text{tem}} = \text{Softmax}(\sigma_{\text{tem}} Q K^T + \mu_{\text{tem}}) V. \quad (4)$$

In this process, Q , K , and V represent the query, key, and value of attention, respectively, each derived from the projection of the input X_{Norm} . The Softmax activation function is applied thereafter. To reverse the spatial patterns before inputting features into the spatial layers, we aim to de-normalize the features of nodes X_{tem} to preserve the spatial relations. Since the temporal representation X_{tem} is transformed by the De-stationary attention module, the input statistics μ_X and σ_X cannot be directly applied. As illustrated in Fig. 1 (c), we employ the SFL module to generate de-normalization factors μ_{spa} and σ_{spa} . In detail, we learn the node-wise features of the original input time series X and the temporal representation X_{tem} using a 1-dimensional convolution on the temporal dimension and a Linear layer. Additionally, the statistics μ_X and σ_X are processed through a linear layer for feature dimension alignment. Subsequently, we utilize a MLP to integrate node-wise features of the input, its temporal representation, and input data statistics to generate the de-normalization factors. Finally, spatial factors μ_{spa} and σ_{spa} are applied to de-normalize X_{tem} .

$$X_{\text{spa}} = \frac{1}{\sigma_{\text{spa}}} X_{\text{tem}} + \mu_{\text{spa}}, \quad (5)$$

where X_{spa} represents the de-normalized result of X_{tem} .

As illustrated in Fig. 2, our framework generates representations whose temporal and spatial distributions closely align with those of the forecasting horizon.

C. Dynamic-Static Fusion Learner

In this section, we propose the DSFL module, which simultaneously captures dynamic and static spatial information and integrates them through an adaptive fusion mechanism. To capture static information for a given task, we employ a trainable task-adaptive node embedding, akin to the approach used in the Adaptive Graph Convolutional Recurrent Network (AGCRN) [57]. Accounting for temporal variations within historical windows, we employ an adaptive node embedding $E_a \in \mathbb{R}^{L \times N \times C}$ to encode the static features of historical time series. Dynamic features are derived from the spatial similarity of each input data through spatial attention mechanisms.

$$A_{\text{Dy}} = Q_{\text{spa}} K_{\text{spa}}^T, \quad (6)$$

$$X_{\text{Dy}} = \text{Softmax}(A_{\text{Dy}}) V_{\text{spa}}, \quad (7)$$

where Q_{spa} , K_{spa} , and $V_{\text{spa}} \in \mathbb{R}^{L \times N \times C}$ represent the value, key, and query of spatial attention, respectively. A_{Dy} represents the adjacency matrix capturing the learned dynamic spatial relations, and X_{Dy} denotes the resulting dynamic features.

TABLE I
DATASETS DETAILS

Attributes	Weather	NYCBike1	NYCBike2	NYCTaxi	PeMS04	PeMS08
Start time	1/1/2012	1/4/2014	1/7/2016	1/1/2015	1/1/2018	1/7/2016
End time	31/12/2022	30/9/2014	29/8/2016	1/3/2015	28/2/2018	31/8/2016
Sample rate	1 hour	30 minutes	30 minutes	30 minutes	5 minutes	5 minutes
Training set	5,623	3,023	1,912	1,912	10,181	10,700
Testing set	1,607	864	546	546	3,394	3,566
Validation set	803	431	274	274	3,394	3,566
Node number	263	128	200	200	307	170
Feature number	1	2	2	2	1	1
Input length	24	19	35	35	12	12
Output length	12	1	1	1	12	12

Then, we extract static features through graph aggregation. In this process, we utilize a fully dense adjacency matrix, $\mathbf{A}_{\text{St}} \in \mathbb{R}^{L \times N \times N}$, derived from the adaptive node embedding \mathbf{E}_a , to depict the spatial relations.

$$\mathbf{A}_{\text{St}} = \mathbf{E}_a \mathbf{E}_a^T, \quad (8)$$

$$\mathbf{X}_{\text{St}} = \mathbf{A}_{\text{St}} \mathbf{X}_{\text{spa}} \mathbf{W}, \quad (9)$$

where $\mathbf{W} \in \mathbb{R}^{C \times C}$ is the parameter matrix, and \mathbf{X}_{St} represents the features learned from static relations.

As the relationships between static and dynamic features change over time, we utilize a gating mechanism to integrate these features. The gate signal z is generated to control the balance between dynamic and static features.

$$\mathbf{X}_{\text{Cat}} = \text{FC}_{\text{Cat}}(\mathbf{X}_{\text{Dy}}, \mathbf{X}_{\text{St}}), \quad (10)$$

$$z = \text{Sigmoid}(\text{FC}(\mathbf{X}_{\text{Cat}})), \quad (11)$$

$$\mathbf{X}_{\text{D}} = z \odot \text{FC}(\mathbf{X}_{\text{Dy}}) + (1 - z) \odot \text{FC}(\mathbf{X}_{\text{St}}), \quad (12)$$

where FC_{Cat} conducts concatenation operation on the last dimension of dynamic features \mathbf{X}_{Dy} and static features \mathbf{X}_{St} , generating the concatenated features $\mathbf{X}_{\text{Cat}} \in \mathbb{R}^{L \times N \times 2C}$. We generate the gate signal z by applying a FC layer to map \mathbf{X}_{Cat} from $\mathbb{R}^{L \times N \times 2C}$ to $\mathbb{R}^{L \times N \times C}$, followed by a Sigmoid activation function; here, FC denotes the fully connected layer. Finally, we employ Equation (12) to fuse the dynamic and static features, producing the final deterministic features \mathbf{X}_{D} , which represent the final deterministic features learned from the input time series.

D. Stochastic Learner

After obtaining the deterministic features, we utilize both backward and forward VAEs to generate the stochastic parts of the historical and forecasting time series. Firstly, the deterministic features \mathbf{X}_{D} are fed into the latent layers $\text{F}_{\text{lat}}(\cdot)$ to obtain the mean μ_{sto} and standard deviation σ_{sto} of \mathbf{X}_{D} , thereby capturing the distribution of the input data. Then, we sample the latent features z_l from the distribution $\mathcal{N}(\mu_{\text{sto}}, \sigma_{\text{sto}}^2)$. These latent features z_l are then processed through the reconstruction layer $\text{F}_{\text{rec}}(\cdot)$ to map back to the stochastic components of

the time series. The processes for the backward and forward Stochastic Learners are detailed below:

$$\mu_{\text{b},\text{sto}}, \sigma_{\text{b},\text{sto}} = \text{F}_{\text{b},\text{lat}}(\mathbf{X}_{\text{D}}), z_{\text{b},l} \sim \mathcal{N}(\mu_{\text{b},\text{sto}}, \sigma_{\text{b},\text{sto}}^2), \quad (13)$$

$$\mu_{\text{f},\text{sto}}, \sigma_{\text{f},\text{sto}} = \text{F}_{\text{f},\text{lat}}(\mathbf{X}_{\text{D}}), z_{\text{f},l} \sim \mathcal{N}(\mu_{\text{f},\text{sto}}, \sigma_{\text{f},\text{sto}}^2), \quad (14)$$

$$\mathbf{X}_{\text{rec}} = \text{F}_{\text{b},\text{rec}}(z_{\text{f},l}), \quad (15)$$

$$\mathbf{X}_{\text{S}} = \text{F}_{\text{f},\text{rec}}(z_{\text{f},l}), \quad (16)$$

where $\mu_{\text{b},\text{sto}}$ and $\sigma_{\text{b},\text{sto}}$ are the mean and standard deviation of the backward features, respectively, and $\mu_{\text{f},\text{sto}}$ and $\sigma_{\text{f},\text{sto}}$ are those of the forward features. $\text{F}_{\text{b},\text{lat}}$ and $\text{F}_{\text{f},\text{lat}}$ represent the backward and forward latent layers, respectively, while $\text{F}_{\text{b},\text{rec}}$ and $\text{F}_{\text{f},\text{rec}}$ represent the backward and forward reconstruction layers. \mathbf{X}_{rec} denotes the reconstruction of the historical time series, and \mathbf{X}_{S} refers to the stochastic parts of the forecasting time series. To ensure that the Stochastic Learner can effectively capture the input dynamic-related stochastic components, we impose constraints on the learned latent feature distribution and the reconstruction values.

The loss function \mathcal{L} consists of three components: prediction error $\mathcal{L}_{\text{pred}}$, reconstruction error \mathcal{L}_{rec} , and the distribution error computed using KL divergence \mathcal{L}_{kl} .

$$\mathcal{L} = \mathcal{L}_{\text{pred}}(\mathbf{X}_{t:t+H}, \hat{\mathbf{X}}_{t:t+H}) + \alpha \mathcal{L}_{\text{rec}}(\mathbf{X}_{t-L:t-1}, \hat{\mathbf{X}}_{t-L:t-1}) + \beta \mathcal{L}_{\text{kl}}, \quad (17)$$

where α and β are hyperparameters that balance the importance of various loss functions, and $\hat{\mathbf{X}}$ represents the time series generated by the neural network. Both the prediction error $\mathcal{L}_{\text{pred}}$ and the reconstruction error \mathcal{L}_{rec} are computed using the Mean Absolute Error (MAE).

After obtaining the deterministic component \mathbf{X}_{D} and the stochastic component \mathbf{X}_{S} of the time series, we input them into the decoder to map the features to the forecasting results. In this paper, the decoder comprises stacks of fully connected (FC) layers.

$$\hat{\mathbf{X}}_{t-L:t} = \text{Decoder}(\text{Concatenate}[\mathbf{X}_{\text{D}}, \mathbf{X}_{\text{S}}]). \quad (18)$$

IV. EXPERIMENTAL SETUPS

In this section, we detail our experimental setup, including the datasets used, the hyperparameter settings for our networks, the baseline comparisons, and the training process.

TABLE II
BASELINE METHODS.

Task type	Methods	Task adaptive	Dynamic adaptive
Time series forecasting	Dual-stage Attention-based Recurrent Neural Network (DA-RNN) [69]	✗	✗
	InfoTS [70]	✓	✓
	AutoTCL [71]	✓	✓
Spatio-temporal forecasting	Temporal Graph Convolutional Network (TGCN) [26]	✗	✗
	Spatio-Temporal Graph Convolutional Network (STGCN) [27]	✗	✗
	Graph Convolutional Gate Recurrent Unit (GCGRU) [28]	✗	✗
	Adaptive Graph Convolutional Recurrent Network (AGCRN) [57]	✓	✗
	Attention based Spatio-Temporal Graph Convolutional Networks (ASTGCN) [72]	✗	✓
	Diffusion Convolutional Recurrent Neural Network (DCRNN) [73]	✗	✗
	Spatio-Temporal Adaptive Embedding transformer (STAEformer) [30]	✓	✓
	Spatio-Temporal Self-Supervised Learning (ST-SSL) [20]	✗	✓
	Meta-Graph Convolutional Recurrent Network (MegaCRN) [74]	✓	✓
	Regularized Graph Structure Learning (RGSL) [16]	✓	✗
	Time-Enhanced Spatio-Temporal Attention Model (TESTAM) [75]	✓	✓
	Memory-based Drift Adaptation network (MemDA) [76]	✓	✓
Ours		✓	✓

TABLE III
THE SELECTION OF α .

Weather		NYCBike1		NYCBike2		NYCTaxi		PeMS04		PeMS08	
α	MAE	α	MAE	α	MAE	α	MAE	α	MAE	α	MAE
0.30	0.765	1.50	5.115	1.00	4.903	1.50	10.961	0.50	19.283	0.50	13.884
0.50	0.719	3.50	5.073	1.50	4.875	2.50	11.039	0.70	18.614	0.70	13.879
0.80	0.705	5.50	5.158	2.50	4.914	3.50	10.864	0.90	18.585	0.90	13.933
1.00	0.660	7.50	5.057	3.50	4.827	4.50	11.074	1.00	18.561	1.00	13.726
3.00	0.766	9.50	5.159	4.50	4.847	5.50	11.030	2.00	18.615	1.20	13.696
β	MAE	β	MAE	β	MAE	β	MAE	β	MAE	β	MAE
0.10	0.670	0.10	5.390	0.10	5.130	0.10	11.264	0.10	32.290	0.10	20.790
0.50	0.665	0.50	5.269	0.50	4.910	0.50	10.758	0.50	25.774	0.50	13.818
1.00	0.664	1.00	5.173	1.00	4.866	1.00	11.136	1.00	18.585	1.00	13.717
5.00	0.658	5.00	4.982	5.00	5.025	5.00	11.114	5.00	18.545	5.00	13.822
10.00	0.672	10.00	5.303	10.00	4.938	10.00	11.161	10.00	18.387	10.00	13.696

A. Datasets

We conduct spatio-temporal forecasting tasks on weather and traffic systems to predict temperature and traffic flows.

Weather datasets. For temperature forecasting, we use the ERA5 hourly dataset [77], originally with a resolution of 0.25° , which we resample to 1° . Our study focuses on an area between 23°N to 35°N latitude and 100°E to 122°E longitude, encompassing 263 nodes. The dataset covers the period from January 1, 2012, to December 31, 2022, and uses historical 24-hour temperature data to predict temperatures 12 hours ahead, with an input interval of 12 hours.

NYC datasets. We use traffic flow datasets for bikes and taxis in New York, which have been preprocessed by Ji *et al.* [20]. These datasets are segmented into three categories: NYCbike1, NYCbike2, and NYCTaxi, recording inflows and outflows of city bikes and taxis every 30 minutes. The NYCbike1 dataset spans from April 1st, 2014, to September 30th, 2014. The NYCbike2 dataset covers the period from July 1st, 2016, to August 29th, 2016, while the NYCTaxi dataset ranges from January 1st, 2015, to March 1st, 2015. The input and output setups are consistent with those described in Ji *et al.* [20]. In NYCbike1, we predict the inflow and outflow of 128

grids 30 minutes ahead using historical records of 9.5 hours, with a sequence length of 19. In NYCBike2 and NYCTaxi datasets, we utilize historical time series of 17.5 hours, with a sequence length of 35. The number of grids in NYCBike2 and NYCTaxi datasets is 200.

PeMS04 and PeMS08 datasets. The PeMS04 and PeMS08 datasets are subsets of the PeMS (PeMS Traffic Monitoring) dataset [78], which includes real-time traffic flow data collected from loop detectors on California highways. Specifically, PeMS04 contains traffic flow records from the San Francisco Bay Area, covering the period from January 1, 2018, to February 28, 2018. PeMS08 encompasses traffic data from July 1, 2016, to August 31, 2016. Both datasets are sampled at 5-minute intervals. In our forecasting task, we aim to predict traffic flow one hour ahead based on the past one-hour records. Both the input and output lengths for each prediction task are set to 12 time steps.

Application features of these datasets are shown in Table I.

B. Training Details

After the exploration stage, the averaged hyperparameters—assumed consistent across benchmarks—are presented

as follows: The dimension C of the adaptive node embedding is 80, consistent with STAEformer [30]. Two-layer MLPs with a hidden dimension of 64 are employed to generate μ_{tem} and σ_{tem} . In the SFL module, the Conv1d layers are configured with an input channel equal to the length of the lookback window L , an output channel of 1, a kernel size of 3, and "circular padding" as defined in the PyTorch package. The Linear layers map the feature dimension to a hidden dimension of 64. For the DSFL module, both the de-stationary attention and spatial attention layers are set to 3. Each de-stationary attention module follows the parameter setup of STAEformer [30], with 4 attention heads and a feed-forward dimension of 256. In the DSFL module, the feature dimensions of X_{Dy} and X_{St} are both set to 160, and the number of attention heads for X_{Dy} is also set to 4. In the Stochastic Learner, the latent layers include 3 Linear layers with ReLU activation functions, mapping the features to 64 dimensions. The reconstruction part of the Stochastic Learner consists of 3 Linear layers followed by ReLU activation functions, which remap the feature dimension from 64 to 160. The decoder comprises 2 Linear layers that fuse the deterministic and stochastic representations to produce the target feature outputs. The balance hyperparameters α and β are fine-tuned experimentally to account for the stochastic nature and uncertainties of the datasets. Table III presents the variation in prediction error corresponding to different values of α , with the value minimizing the error selected as optimal. Moreover, the training process is conducted on the Adam optimizer with a learning rate of 0.001 and a batch size of 32. The number of training epochs is set to 100. We split the datasets into training, validation and test set with a ratio shown in Table I. Numerical experiments for the methods are conducted using various random seeds from the set $\{31, 32, 33, 34, 35\}$ to obtain the average performance and standard deviation.

C. Baselines

We compare our method against several baseline approaches, including state-of-the-art multi-variable time series forecasting methods and spatio-temporal forecasting methods. Spatio-temporal forecasting techniques can be classified into two categories based on how they learn spatial relations: task-adaptive and dynamic-adaptive methods. Task-adaptive methods focus on learning static temporal and spatial relations from training datasets, which remain fixed during the testing phase. In contrast, dynamic-adaptive methods capture dynamically changing relations from input windows or by updating memory with incoming data. Details of the baseline methods are provided in Table II. In multi-variable time series forecasting, DA-RNN is a classic dual-stage attention-based recurrent neural network designed to capture long-term temporal dependencies. InfoTS and AutoTCL focus on enhancing time series representation learning through series augmentations and contrastive learning. InfoTS introduces a novel contrastive learning approach with information-aware augmentations that adaptively select optimal augmentations and a meta-learner network to learn from datasets. AutoTCL achieves unified and meaningful time series augmentations at both the dataset

and instance levels, leveraging information theory to enhance representation quality. TGCN, STGCN, DCRNN and GCGRU utilize physical spatial relations as adjacency matrices and employ static neural networks for prediction. TGCN, DCRNN, and GCGRU use Graph Convolutional Networks (GCN) and Recurrent Neural Networks (RNN) to capture spatial and temporal features. STGCN combines temporal and graph convolutions to learn spatial and temporal dependencies. AGCRN utilizes learnable node embeddings to adapt spatial relations to tasks and node-adaptive parameters to capture specific attributes of each node. ASTGCN and STAEformer employ attention mechanisms to capture dynamic changes in input features. RGSL learns spatio-temporal dependencies from a predefined graph and learnable node embeddings, dynamically fusing features from two graphs using an attention mechanism. Additionally, STAEformer employs learnable node embeddings and concatenates it with input time series to capture static features. MegaCRN utilizes node embeddings to learn the static relations and memory networks to dynamically match sample patterns with learned static features. ST-SSL does not learn static relations and only uses the adjacency matrix based on node distances as a prior graph. It fine-tunes the static graph using node similarities, effectively fusing dynamic and static features. TESTAM employs a mixture-of-experts model with three experts: one for temporal modeling, one for spatio-temporal modeling with a static graph, and one for spatio-temporal dependency modeling with a dynamic graph. **We also fine-tune the hyperparameters of baseline methods to ensure fairness, especially for datasets not included in their official implementations.** We evaluate the performance of these models using two metrics: MAE and Mean Absolute Percentage Error (MAPE). The number of samples in the test datasets is denoted as m . $\hat{\mathbf{X}}$ and \mathbf{X} denote the predicted and actual observations of spatio-temporal systems.

$$\text{MAE} = \frac{1}{m} \sum_{j=1}^m |\hat{\mathbf{X}} - \mathbf{X}|, \quad (19)$$

$$\text{MAPE} = \frac{100\%}{m} \sum_{j=1}^m \left| \frac{\hat{\mathbf{X}} - \mathbf{X}}{\mathbf{X}} \right|. \quad (20)$$

V. EXPERIMENTAL RESULTS

A. Comparison Results

As shown in Tables IV and V, numerical experiments, present the average performance and standard deviation of both the baseline methods and our DRAN model. Our DRAN model outperforms the baseline methods, demonstrating the best overall performance. DRAN achieves the best average performance on the Weather and NYC datasets, **and ranks second on the PeMS04 and PeMS08 datasets.** Our method performs less effectively on the MAPE metric but excels on the MAE metric. This suggests that the model prioritizes optimizing the overall error rather than minimizing relative error in specific scenarios, such as scenarios with small target values. Consequently, while DRAN's performance on the MAPE metric is slightly lower than that of other methods, its

TABLE IV
THE PREDICTION RESULTS ON WEATHER AND NYC DATASETS.

Methods & Metrics	Datasets	Weather		NYCBike1		NYCBike2		NYCTaxi	
		Temperature	Inflow	Outflow	Inflow	Outflow	Inflow	Outflow	
DA-RNN [69]	MAE	7.951 \pm 1.036	14.158 \pm 3.523	14.565 \pm 3.383	13.192 \pm 1.014	13.115 \pm 1.178	24.642 \pm 7.398	28.721 \pm 8.953	
	MAPE (%)	2.709 \pm 0.355	60.359 \pm 12.515	62.955 \pm 12.885	53.894 \pm 4.686	60.253 \pm 13.219	67.319 \pm 9.888	70.737 \pm 14.281	
InfoTS [70]	MAE	1.343 \pm 0.031	6.436 \pm 0.133	6.797 \pm 0.138	6.641 \pm 0.091	6.087 \pm 0.096	14.912 \pm 0.239	11.545 \pm 0.225	
	MAPE (%)	0.459 \pm 0.011	33.724 \pm 0.553	34.920 \pm 0.551	32.231 \pm 0.634	30.113 \pm 0.603	21.770 \pm 0.442	20.982 \pm 0.409	
AutoTCL [71]	MAE	1.194 \pm 0.025	6.002 \pm 0.037	6.424 \pm 0.034	6.011 \pm 0.060	5.533 \pm 0.063	14.843 \pm 0.162	11.394 \pm 0.095	
	MAPE (%)	0.408 \pm 0.008	28.076 \pm 0.201	29.573 \pm 0.164	29.512 \pm 0.380	27.766 \pm 0.409	22.061 \pm 0.189	21.140 \pm 0.136	
STGCN [27]	MAE	2.278 \pm 1.103	17.106 \pm 0.016	17.177 \pm 0.216	32.981 \pm 35.614	30.180 \pm 28.265	78.624 \pm 40.578	65.907 \pm 33.232	
	MAPE (%)	0.778 \pm 0.377	58.208 \pm 1.926	58.789 \pm 1.383	63.402 \pm 19.134	62.237 \pm 13.177	84.124 \pm 30.571	75.094 \pm 24.967	
TGCN [26]	MAE	1.736 \pm 0.847	7.412 \pm 0.052	7.677 \pm 0.441	6.103 \pm 0.106	5.712 \pm 0.072	25.307 \pm 11.321	21.715 \pm 9.109	
	MAPE (%)	0.592 \pm 0.287	34.611 \pm 0.827	35.085 \pm 1.704	29.717 \pm 0.592	28.286 \pm 0.632	44.536 \pm 10.924	45.181 \pm 10.584	
MemDA [76]	MAE	1.786 \pm 0.071	6.777 \pm 0.154	7.246 \pm 0.100	6.452 \pm 0.127	6.284 \pm 0.252	18.505 \pm 0.661	17.199 \pm 0.542	
	MAPE (%)	0.611 \pm 0.026	29.344 \pm 0.543	30.351 \pm 0.126	29.312 \pm 0.571	27.995 \pm 0.802	28.719 \pm 1.861	32.463 \pm 1.726	
ASTGCN [72]	MAE	1.521 \pm 0.155	6.481 \pm 0.352	6.698 \pm 0.541	6.658 \pm 0.326	7.548 \pm 3.533	15.389 \pm 5.711	12.500 \pm 3.923	
	MAPE (%)	0.520 \pm 0.054	30.780 \pm 1.221	31.264 \pm 1.976	28.674 \pm 1.021	27.028 \pm 1.123	24.731 \pm 0.916	24.443 \pm 1.578	
TESTAM [75]	MAE	1.481 \pm 1.203	6.331 \pm 0.736	6.826 \pm 0.891	6.437 \pm 0.852	6.266 \pm 0.901	17.684 \pm 1.814	15.967 \pm 2.758	
	MAPE (%)	0.507 \pm 0.415	30.418 \pm 2.571	31.628 \pm 2.949	28.565 \pm 3.457	27.762 \pm 2.620	25.703 \pm 3.433	25.988 \pm 4.105	
AGCRN [57]	MAE	1.094 \pm 0.039	5.066 \pm 0.020	5.366 \pm 0.023	5.279 \pm 0.058	4.941 \pm 0.035	12.263 \pm 0.132	9.720 \pm 0.098	
	MAPE (%)	0.373 \pm 0.013	25.551 \pm 0.200	26.564 \pm 0.209	25.498 \pm 0.268	24.633 \pm 0.286	18.234 \pm 0.324	18.239 \pm 0.278	
GCGRU [28]	MAE	1.012 \pm 0.041	5.457 \pm 0.063	5.631 \pm 0.290	5.313 \pm 0.064	4.987 \pm 0.056	12.153 \pm 2.649	10.277 \pm 1.340	
	MAPE (%)	0.346 \pm 0.015	26.867 \pm 0.700	27.292 \pm 1.476	25.428 \pm 0.423	24.490 \pm 0.185	22.386 \pm 7.043	22.800 \pm 7.607	
DCRNN [73]	MAE	0.984 \pm 0.028	5.374 \pm 0.039	5.557 \pm 0.305	5.386 \pm 0.036	5.047 \pm 0.031	12.097 \pm 3.639	9.833 \pm 2.314	
	MAPE (%)	0.336 \pm 0.010	26.772 \pm 0.850	27.165 \pm 1.507	25.279 \pm 0.273	24.332 \pm 0.164	21.182 \pm 3.214	21.598 \pm 3.360	
STAEformer [30]	MAE	3.728 \pm 2.367	5.168 \pm 0.029	5.475 \pm 0.028	5.453 \pm 0.100	5.112 \pm 0.147	12.262 \pm 0.237	9.824 \pm 0.109	
	MAPE (%)	1.284 \pm 0.819	25.829 \pm 0.331	26.889 \pm 0.242	25.774 \pm 0.429	24.840 \pm 0.447	17.889 \pm 0.777	18.203 \pm 0.684	
MegaCRN [74]	MAE	0.952 \pm 0.027	5.042 \pm 0.016	5.357 \pm 0.043	5.152 \pm 0.049	4.826 \pm 0.021	12.084 \pm 0.158	9.569 \pm 0.175	
	MAPE (%)	0.325 \pm 0.010	25.329 \pm 0.167	26.275 \pm 0.213	24.878 \pm 0.409	23.870 \pm 0.293	17.883 \pm 0.204	17.664 \pm 0.338	
RGSL [16]	MAE	0.727 \pm 0.003	5.149 \pm 0.140	5.335 \pm 0.200	5.251 \pm 0.039	4.915 \pm 0.060	12.083 \pm 0.125	9.582 \pm 0.072	
	MAPE (%)	0.248 \pm 0.001	25.612 \pm 0.183	26.110 \pm 0.924	24.186 \pm 2.957	23.288 \pm 2.249	18.430 \pm 0.531	18.205 \pm 0.319	
ST-SSL [20]	MAE	1.352 \pm 0.010	5.135 \pm 0.024	5.265 \pm 0.023	5.042 \pm 0.029	4.714 \pm 0.023	12.010 \pm 0.481	9.790 \pm 0.101	
	MAPE (%)	0.461 \pm 0.004	25.430 \pm 0.295	24.605 \pm 0.265	22.633 \pm 0.112	21.813 \pm 0.808	16.383 \pm 0.100	16.855 \pm 0.228	
Ours	MAE	0.672 \pm 0.007	4.882 \pm 0.032	5.176 \pm 0.054	5.008 \pm 0.056	4.653 \pm 0.036	11.929 \pm 0.054	9.539 \pm 0.054	
	MAPE (%)	0.229 \pm 0.002	23.553 \pm 0.169	24.607 \pm 0.497	22.384 \pm 0.211	21.429 \pm 0.208	16.338 \pm 0.409	16.666 \pm 0.201	

Results with **bold** are the overall best performance, and **shading** results have the suboptimal performance.

superior MAE results demonstrate effective overall error control. In terms of prediction stability, DRAN exhibits slightly larger standard deviations compared to other methods across experiments with different random seeds. This is likely due to the model's attempt to learn noise components in the representation, which are randomly sampled from distributions.

ST-SSL exhibits strong performance in one-step traffic flow prediction but is less effective on other datasets. This discrepancy may be due to ST-SSL's emphasis on one-step ahead prediction, as its decoder is not optimized for multi-step forecasting. Additionally, MegaCRN performs well across both tasks, likely due to its task-adaptive node embeddings and the dynamic features learned from its meta memory networks. RGSL benefits from dynamically fusing an explicit prior graph with a learned implicit graph using attention mechanisms. STAEformer performs well on some datasets but poorly on others, which may be attributed to its non-adaptive fusion process. These results suggest that our proposed DRAN model is capable of adapting to various tasks and effectively capturing

both static and dynamic features.

Furthermore, we display the prediction results of our DRAN and the sub-optimal methods. As is shown in Fig. 3, by comparing the prediction errors of our DRAN, RGSL, and MegaCRN, we find that while the numerical metrics of these methods are very close, the distribution of prediction errors is different. The prediction results of our method demonstrate a more stable performance across all spatial regions, whereas other methods exhibit significantly larger errors in certain regions. This indicates that our method is more stable in prediction and better adapts to nodes with complex dynamic changes. As shown in Fig. 4, we provide two cases as examples to visualize the prediction results. We can see that both methods generate predictions that are similar to the ground truth. However, when comparing spatial prediction errors, DRAN shows fewer grids with large prediction errors. Additionally, we present the predicted time series of nodes in Fig. 5. In the weather dataset, both RGSL and our method capture the overall temporal trends of nodes and perform

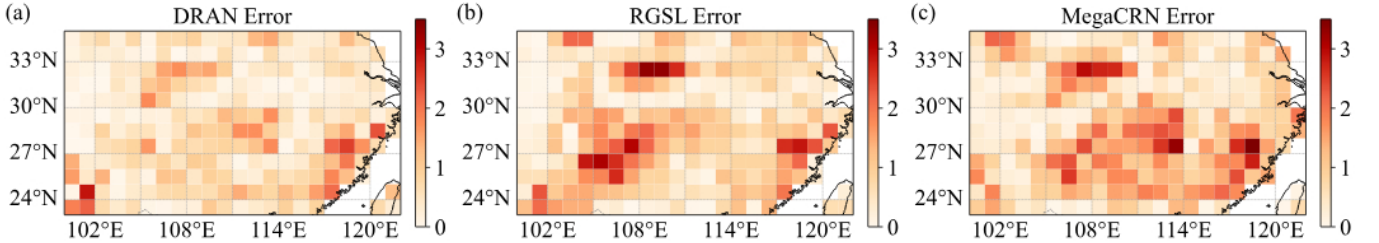


Fig. 3. Prediction errors for the weather dataset. (a), (b), and (c) show the absolute prediction errors for DRAN, RGSL, and MegaCRN, respectively.

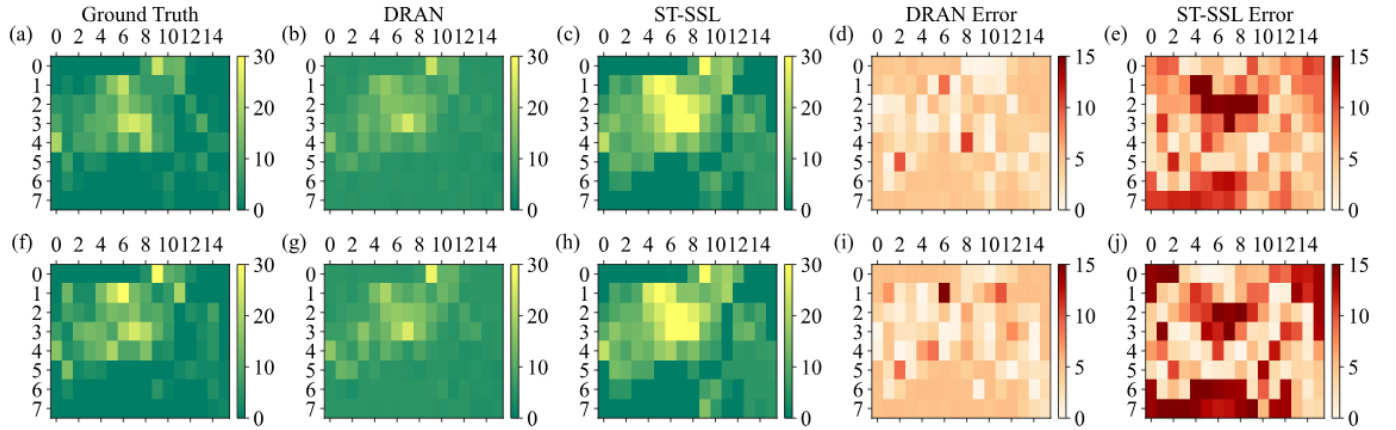


Fig. 4. Prediction results for the NYCBike1 dataset. The city is partitioned into a grid map. Panels (a) and (f) in the first column show the actual bike flow, while panels (b) and (g) display the predictions made by our DRAN model. Panels (c) and (h) present the predictions from the sub-optimal method ST-SSL. Panels (d) and (i) illustrate the absolute prediction errors for DRAN, and panels (e) and (j) depict the absolute prediction errors for ST-SSL.

well in the more regular periodic variations, though they lack accuracy in some extreme values. This may be due to an insufficient ability to capture abrupt changes in the time series. In Fig. 5 (c) and (d), DRAN demonstrates superior performance in predicting the sudden decrease in traffic flow.

To balance computational cost and prediction accuracy, we compare inference times in Table VI, where methods are listed in descending order of inference time. The comparison is conducted using input data of the same size, repeated 100 times to compute the average inference time for a batch of NYCTaxi data. All experiments are performed on an Nvidia RTX3090 GPU. While DA-RNN achieves the fastest inference speed, it lacks sufficient prediction accuracy. DRAN delivers the best prediction accuracy with a moderate latency at inference time, comparable to ST-SSL and STAEformer.

B. The Preservation of Spatial Distribution

To evaluate whether the SFL module preserves spatial distributions across various tasks or not, we analyze the spatial distributions of representations before SFL (\mathbf{X}_{tem}), after SFL (\mathbf{X}_{spa}), and at the forecasting horizon ($\mathbf{X}_{t:t+H}$). The objective is to determine whether the distributions of representations after SFL are closer to those at the forecasting horizon. For each forecasting task, we randomly generate indices and select samples from \mathbf{X}_{tem} , \mathbf{X}_{spa} , and $\mathbf{X}_{t:t+H}$. We then use Gaussian Kernel Density Estimation to assess the distributions of these representations. As visualized in Fig. 6, the results demonstrate the SFL module's ability to preserve the spatial

distribution of nodes. The primary goal of SFL is to align the spatial distribution of learned representations with that of the forecasting horizon, thereby enhancing accuracy in capturing spatial and temporal distribution changes. In Fig. 6, significant discrepancies between the spatial distribution of representations before SFL and the final horizon are observed. The SFL module effectively reduces these variations in the spatial distributions of learned representations, thereby facilitating the learning process to map spatially preserved representations to predictions.

Furthermore, we replace the temporal normalization modules to verify the effectiveness of SFL across various temporal normalization operations. We assessed SFL's ability to preserve spatial distribution when combined with different temporal normalization modules: DAIN, Dish-TS, the Non-stationary Transformer and ST-norm. DAIN utilizes MLPs and a gate mechanism to learn the adaptive mean and standard deviation of input time series. The Non-stationary Transformer normalizes the time series and employs scaling factors to prevent removing excessive temporal information within the attention module. Dish-TS normalizes and de-normalizes the lookback horizon windows using different learned means and standard deviations. We applied temporal normalization after the frequency cutting operation, with SFL using the mean and standard deviation of the lookback windows to generate spatial factors. Given that RevIN performs normalization on feature dimensions, we conducted experiments applying only feature normalization to investigate whether this coarse-grained ap-

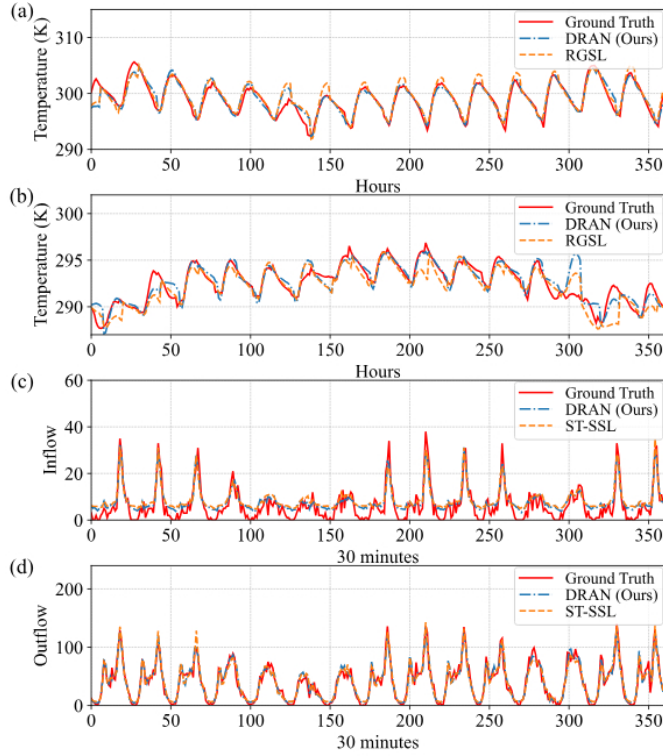


Fig. 5. Visualization of temporal prediction results. (a) and (b) display the predicted temperature of Weather dataset of node 20 and node 190 from November 3rd, 2020 to November 17th, 2019. (c) and (d) show the predicted traffic inflow and outflow of NYC Bike1 dataset of node 50 from 0:00 of August 25th, 2014 to 12:00 of September 1st.

proach, which simultaneously normalizes both spatial and temporal distributions, is sufficient for spatio-temporal forecasting tasks. ST-norm applies spatial and temporal normalization to the inputs, enabling the model to better capture high-frequency spatial features and local temporal features. We compare three scenarios: applying T-norm only, applying ST-norm, and combining T-norm with the SFL module.

As shown in Table VII, SFL improves the performance of various temporal normalization methods, demonstrating its effectiveness as a general module for spatial distribution preservation. The models incorporating temporal operations and SFL outperform the model with RevIN. This finding suggests that normalization on feature dimensions alone is too coarse-grained and may not be adequate for distribution adaptation in spatio-temporal tasks. In ST-norm, the combination of spatial and temporal normalization improves performance. However, combining T-norm with the SFL module results in greater accuracy improvement, suggesting that the rescaling spatial distributions contribute more significantly to imitating propagation dynamics than normalization alone. Therefore, SFL after temporal normalization is an effective approach for distribution adaptation compared with instance-level and spatial and temporal level normalization.

C. Dynamic and Static Relations Learning

In Fig. 7, we explore the adaptive process of our model by depicting the dynamic and static adjacency matrices within

TABLE V
THE PREDICTION RESULTS ON PEMSO4 AND PEMSO8 DATASETS.

Methods & Metrics	Datasets	PeMS04 Flow	
		PeMS04 Flow	PeMS08 Flow
DA-RNN [69]	MAE MAPE (%)	104.741±12.184 137.640±18.494	92.276±9.643 66.774±13.187
InfoTS [70]	MAE MAPE (%)	25.851±0.510 19.556±0.464	24.006±1.225 14.682±0.666
AutoTCL [71]	MAE MAPE (%)	23.814±0.048 20.879±0.098	17.355±0.200 13.006±0.121
TGCN [26]	MAE MAPE (%)	34.785±0.204 27.972±0.754	24.448±0.129 14.589±0.219
GCGRU [28]	MAE MAPE (%)	24.398±0.043 15.105±0.464	17.778±3.356 10.622±2.838
STGCN [27]	MAE MAPE (%)	25.302±2.316 24.321±8.603	25.338±10.825 15.404±7.083
DCRNN [73]	MAE MAPE (%)	24.912±2.064 17.720±0.973	20.853±0.062 11.864±0.094
ASTGCN [72]	MAE MAPE (%)	23.565±0.942 16.813±1.004	20.195±0.398 11.303±0.552
ST-SSL [20]	MAE MAPE (%)	22.836±0.705 14.318±0.435	18.559±0.097 10.615±0.122
MemDA [76]	MAE MAPE (%)	20.037±0.150 11.969±0.100	16.370±0.207 9.342±0.243
RGSL [16]	MAE MAPE (%)	19.544±0.2571 13.862±0.242	17.452±3.102 9.186±0.182
TESTAM [75]	MAE MAPE (%)	19.331±0.481 12.098±0.419	15.757±0.360 9.083±0.215
AGCRN [57]	MAE MAPE (%)	19.3291±0.3053 12.937±0.035	16.101±0.085 9.219±0.065
MegaCRN [74]	MAE MAPE (%)	18.858±0.0413 12.808±0.098	15.597±0.245 8.834±0.096
STAEformer [30]	MAE MAPE (%)	18.241±0.082 12.064±0.071	13.538±0.039 8.858±0.017
Ours	MAE MAPE (%)	18.375±0.087 12.026±0.419	13.690±0.085 8.987±0.057

Results with **bold** are the overall best performance, and **shading** results have the suboptimal performance.

the DSFL module. Specifically, we showcase these matrices for the first input time step as an example. The dynamic adjacency matrix A_{Dy} is derived from the similarity of time series between nodes according to Equation 6, while the static adjacency matrix is obtained by learning the static relations A_{St} according to Equation 8. Fig. 7 illustrates the spatial relations between nodes of Weather dataset, with darker colors indicating stronger relationships. The dynamic adjacency matrix highlights the strength of relationships between nodes with similar signal patterns, whereas the static adjacency matrix focuses on the signals of individual nodes and some distributed nodes within the network. **The contrast in focus enables the model to learn complementary features from both dynamic and static perspectives.**

To clarify the differences between the learned dynamic and static relations for specific nodes, we select node i from various locations and visualize the relationships between the selected node and other nodes, represented as $A_{St,i}$ and $A_{Dy,i}$. As shown in Fig. 8, subfigures (a), (b), and (c) depict the dynamic

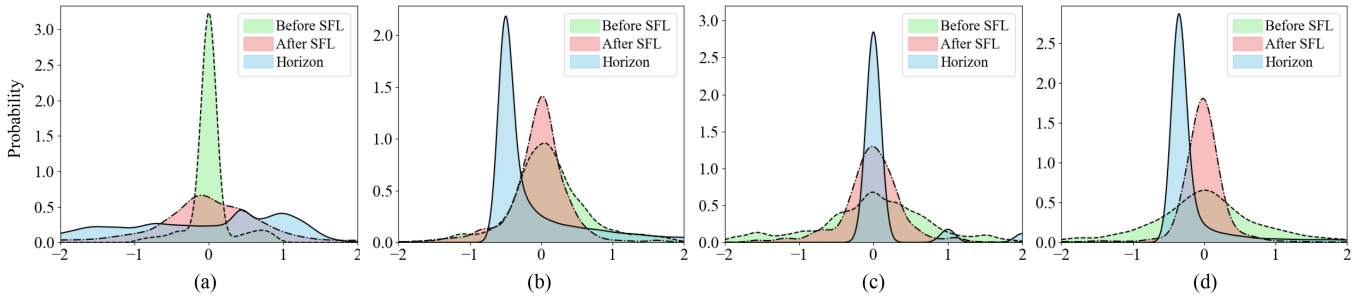


Fig. 6. The preservation of spatial distribution by the SFL module across the Weather, NYCBike1, NYCBike2, and NYCTaxi datasets is illustrated in panels (a), (b), (c), and (d). These panels showcase changes in the spatial distribution of latent representations and forecasting horizons. "Before SFL", "After SFL", and "Horizon" denote the spatial distribution of representations before the SFL module \mathbf{X}_{tem} , after the SFL module \mathbf{X}_{spa} , and at the forecasting horizon $\mathbf{X}_{t:t+H}$, respectively.

TABLE VI
INFERENCE TIME COMPARISON

Methods	Time (s)	MAE
GConvGRU [28]	1.383	12.022
DCRNN [73]	0.967	11.924
TGCN [26]	0.469	28.475
STGCN [27]	0.343	12.286
RGSL [16]	0.246	10.833
InfoTS [70]	0.179	13.228
MegaRCN [74]	0.178	10.827
AGCRN [57]	0.126	10.992
ASTGCN [72]	0.114	14.422
TESTAM [75]	0.075	16.826
DRAN (Ours)	0.075	10.734
ST-SSL [20]	0.073	10.996
STAformer [30]	0.065	10.810
MemDA [76]	0.056	17.852
AutoTCL [71]	0.052	13.119
DA-RNN [69]	0.048	26.596

Experiments are conducted on a batch of NYCTaxi data which contains 8 samples. Results with **bold** are the fastest method and the method with best prediction performance.

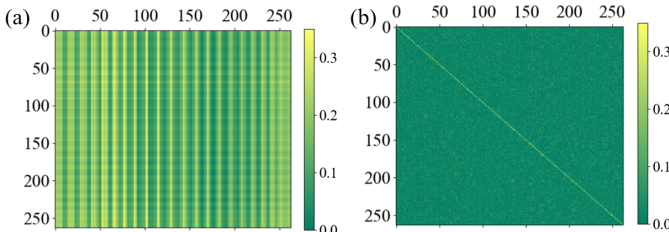


Fig. 7. The dynamic (a) and static (b) adjacency matrices of weather dataset. The larger value indicates a closer relationship between nodes.

relations between target nodes and other nodes in the Weather dataset, while subfigures (d), (e), and (f) illustrate the static relations. The dynamic relations learned by DSFL concentrate around the target nodes, highlighting the significance of local connections. In contrast, the static relations reflect interactions between target nodes and distant nodes, indicating that the static adjacency matrix captures non-local relationships. This demonstrates that DSFL effectively learns comprehensive and non-overlapping spatial relations.

Moreover, the gate mechanism enables adaptive integration of dynamic and static features. We visualize the first channel

of the gate signal z from three layers of DSFL modules in Fig. 9, illustrating fusion ratio variations on the NYCBike2 test set. Each gate mechanism performs hierarchical fusion, where the blue-filled area represents the contribution of static features to the final deterministic features \mathbf{X}_D , and the orange area represents the dynamic features. The fusion ratios vary in sync with the fluctuations of the input inflow and outflow series, demonstrating the gate mechanism's ability to adaptively balance dynamic and static information.

D. Ablation Studies

To evaluate the effectiveness of each module in our network, we conduct an ablation study by systematically removing specific components. Specifically, we remove the DSFL module, the gate mechanism in DSFL module, the SFL module, the entire distribution adaptive module, and the Stochastic Learner to observe the resulting changes in prediction accuracy. The ablation strategies are detailed as follows:

- **w/o Sto:** We remove the Stochastic Learner and used only the deterministic features for prediction. In this case, only \mathbf{X}_D is input into the decoder.
- **w/o Sta:** We remove all modules related to non-stationarity and distribution adaptation, including normalization and de-normalization operations and the SFL module, and replace the de-stationary attention with standard attention [79].
- **w/o SFL:** We remove the SFL module, resulting in a temporal-only normalization similar to that in the non-stationary Transformer.
- **w/o DSFL:** We remove the DSFL module and use spatial attention instead.
- **w/o Gate:** We remove the gate mechanism and replace it with a Linear layer mapping concatenated feature $\mathbf{F}_{\text{Cat}} \in \mathbb{R}^{L \times N \times 2C}$ to shape $\mathbb{R}^{L \times N \times C}$.

The results of the ablation study are depicted in Fig. 10. The final model, incorporating all modules, achieves the best performance. It is evident that the SFL module contributes most significantly to improving prediction accuracy across different tasks. Removing all distribution adaptation modules (w/o Sta) has less impact compared to removing the SFL module (w/o SFL), highlighting SFL as a crucial and indispensable component for spatio-temporal distribution adaptation. The

TABLE VII
THE EFFECTIVENESS OF SFL ON VARIOUS TEMPORAL NORMALIZATION METHODS.

Strategies	Datasets	Weather		NYCBike1		NYCBike2		NYCTaxi	
		Temperature	Inflow	Outflow	Inflow	Outflow	Inflow	Outflow	
+RevIN	MAE	0.732 \pm 0.004	5.031 \pm 0.064	5.341 \pm 0.094	5.192 \pm 0.068	4.831 \pm 0.060	12.301 \pm 0.217	9.714 \pm 0.168	
+DAIN	MAE	1.035 \pm 0.006	5.212 \pm 0.088	5.508 \pm 0.084	5.670 \pm 0.420	5.258 \pm 0.290	13.747 \pm 0.174	10.848 \pm 0.088	
+DAIN+SFL	MAE	0.663 \pm 0.003	4.942 \pm 0.050	5.229 \pm 0.028	5.268 \pm 0.135	4.899 \pm 0.159	12.303 \pm 0.147	9.828 \pm 0.171	
+Non-st	MAE	0.738 \pm 0.006	5.096 \pm 0.109	5.368 \pm 0.089	5.297 \pm 0.073	4.924 \pm 0.072	13.344 \pm 0.051	10.540 \pm 0.159	
+Non-st+SFL	MAE	0.671 \pm 0.006	4.882 \pm 0.032	5.176 \pm 0.054	5.008 \pm 0.056	4.653 \pm 0.036	11.929 \pm 0.054	9.539 \pm 0.054	
+Dish-TS	MAE	0.764 \pm 0.003	5.024 \pm 0.080	5.370 \pm 0.101	5.215 \pm 0.017	4.843 \pm 0.022	12.363 \pm 0.314	9.868 \pm 0.223	
+Dish-TS+SFL	MAE	0.676 \pm 0.008	4.998 \pm 0.094	5.317 \pm 0.079	5.077 \pm 0.050	4.777 \pm 0.053	12.208 \pm 0.208	9.720 \pm 0.133	
+ST-norm	MAE	1.288 \pm 0.038	5.205 \pm 0.069	5.469 \pm 0.072	9.782 \pm 0.526	9.455 \pm 0.500	13.993 \pm 0.621	11.252 \pm 0.529	
+T-norm	MAE	1.712 \pm 0.046	5.291 \pm 0.245	5.556 \pm 0.146	8.876 \pm 0.935	8.704 \pm 0.932	13.469 \pm 0.292	10.788 \pm 0.319	
+T-norm+SFL	MAE	0.747 \pm 0.165	4.952 \pm 0.056	5.239 \pm 0.031	8.479 \pm 0.211	8.204 \pm 0.240	12.149 \pm 0.124	9.654 \pm 0.055	

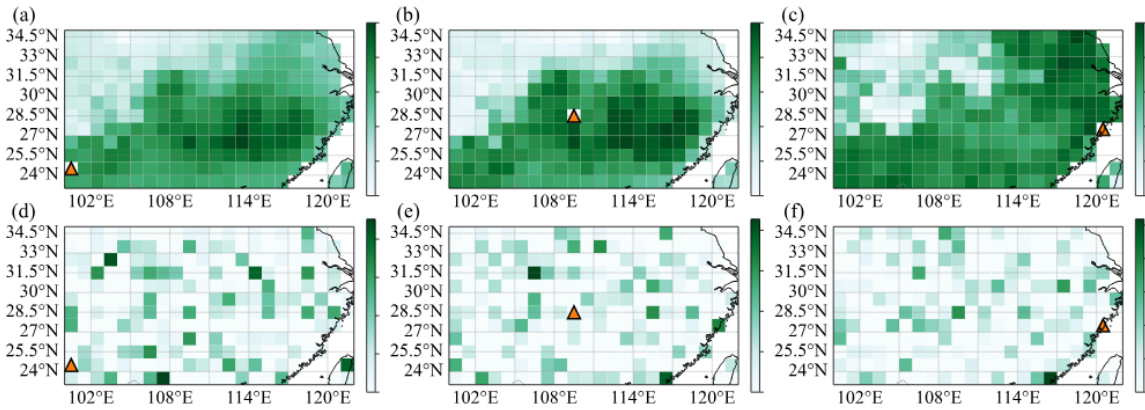


Fig. 8. Visualization of relation strengths for three nodes located in different areas of Weather dataset. The orange triangles represent the selected target nodes. The darker color indicates a closer relationship between nodes. Panels (a), (b), and (c) show the dynamic relations of the nodes, while panels (d), (e), and (f) display the static relations.

effectiveness of the Stochastic Learner varies depending on the task, aligning with the fact that task uncertainties differ. Comparing the experimental results of "w/o Gate" and "w/o DSFL," the prediction error increases more significantly when the gate mechanism in the DSFL module is removed than when the entire DSFL module is removed. This suggests that fusing dynamic and static representations with a fixed ratio, without considering the time-varying relationships between them, hinders accurate prediction and results in an unsuitable feature combination. Moreover, our model outperforms the scenario where all normalization operations are removed, highlighting the necessity of normalization in spatio-temporal data processing.

VI. DISCUSSION AND CONCLUSIONS

From the carried out experiments we can conclude the following:

- The proposed method performs better in the spatio-temporal forecasting task compared with baseline methods at the cost of a moderate computation.
- The proposed SFL module can be inserted with other temporal normalization methods and architectures, adapting distribution shifts in spatio-temporal context.

- The proposed DSFL module is effective to both capture the dynamic and static spatial relations.
- Each component (SFL, DSFL and Stochastic learner) in our DRAN model provides value in prediction accuracy improvements. The adaptive fusion ratio derived from the gate mechanism is important for the integration of static and dynamic features.

Despite its strengths in accuracy performance, the methods suffers in terms of memory requirements and computational resources needs from scalability in large datasets or applications characterized by real-world systems. Additionally, the current design focuses on regular spatio-temporal patterns, making it less effective in scenarios characterized by the presence of abrupt changes or rare events.

To overcome above limitations, future work should focus on:

- **Scalability:** Given the time costs associated with model training and inference, further research should investigate a more lightweight framework to deal with distribution shifts. This approach would improve scalability and enable the model to be effectively applied to large real-world datasets.
- **Adaptability and Transferability:** While our framework currently emphasizes relation and distribution adaptation,

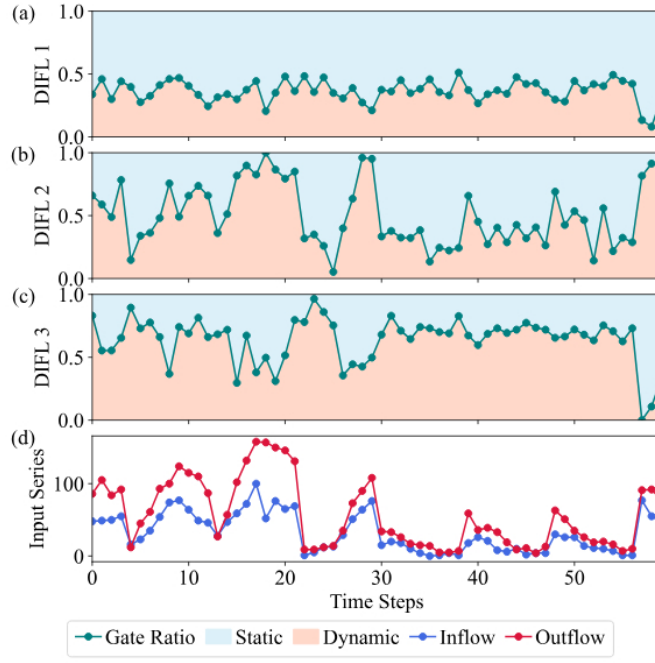


Fig. 9. Gate fusion ratio variations of DSFL modules on the NYCBike2 dataset during the test period. Panels (a), (b), and (c) show the first-channel dynamic and static fusion ratios for three DSFL modules, while panel (d) presents the corresponding input time series of the consistent gate ratios.

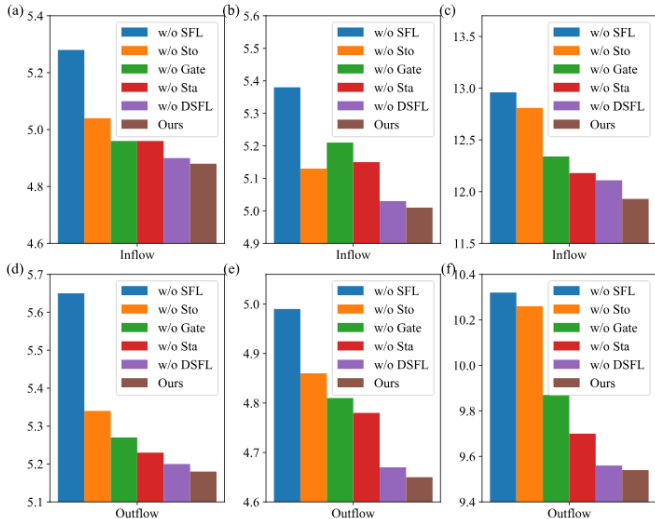


Fig. 10. The results of ablation studies. Panels (a)–(c) show the MAE for inflow prediction, and panels (d)–(f) for outflow prediction, across the NYCBike1, NYCBike2, and NYCTaxi datasets, respectively. Each bar color denotes the removal of a specific module, as indicated in the legend. “Ours” represents the full model.

it lacks mechanisms for dynamically adjusting network parameters based on learned knowledge and new inputs. Future work will focus on developing strategies to learn and update network parameters, drawing inspiration from techniques like EAST-Net [67], which generates sequence-specific, on-the-fly parameters. Enhancing adaptability will enable the model to better detect and respond to sudden changes and events.

VII. CONCLUSION

To conclude, **spatio-temporal** forecasting is essential for understanding the states of complex systems, yet accurate predictions are often hindered by the dynamic and intricate nature of these systems. This study addresses the challenge of adapting to dynamic changes in spatio-temporal systems using neural networks. **A DRAN framework is proposed** to accommodate changes in distribution shifts, relations, and stochastic variations. Our approach includes a SFL to enable effective temporal normalization for spatio-temporal contexts. Additionally, we develop a DSFL to capture features from both dynamic and static relations. Furthermore, our framework enables to learn the deterministic and stochastic representations of features. Experimental results demonstrate the superiority of our method and the effectiveness of its components.

REFERENCES

- [1] C. Peng, T. Tang, Q. Yin, X. Bai, S. Lim, and C. C. Aggarwal, “Physics-informed explainable continual learning on graphs,” *IEEE Transactions on Neural Networks and Learning Systems*, vol. 35, no. 9, pp. 11 761–11 772, 2024.
- [2] T. Liu, D. Chen, L. Yang, J. Meng, Z. Wang, J. Ludescher, J. Fan, S. Yang, D. Chen, J. Kurths, X. Chen, S. Havlin, and H. J. Schellnhuber, “Teleconnections among tipping elements in the earth system,” *Nature Climate Change*, vol. 13, no. 1, pp. 67–74, 2023. [Online]. Available: <https://doi.org/10.1038/s41558-022-01558-4>
- [3] Y. Verma, M. Heinonen, and V. Garg, “ClimODE: Climate and weather forecasting with physics-informed neural ODEs,” in *The Twelfth International Conference on Learning Representations*, 2024. [Online]. Available: <https://openreview.net/forum?id=xuY33XhEGR>
- [4] L. Chen, F. Du, Y. Hu, Z. Wang, and F. Wang, “Swinrdm: Integrate swinrnn with diffusion model towards high-resolution and high-quality weather forecasting,” in *Proceedings of the AAAI Conference on Artificial Intelligence*, vol. 37, no. 1, Jun. 2023, pp. 322–330. [Online]. Available: <https://ojs.aaai.org/index.php/AAAI/article/view/25105>
- [5] A. Gasparin, S. Lukovic, and C. Alippi, “Deep learning for time series forecasting: The electric load case,” *CAAI Transactions on Intelligence Technology*, vol. 7, no. 1, pp. 1–25, 2022.
- [6] L. Xiong, Y. Tang, S. Mao, H. Liu, K. Meng, Z. Dong, and F. Qian, “A two-level energy management strategy for multi-microgrid systems with interval prediction and reinforcement learning,” *IEEE Transactions on Circuits and Systems I: Regular Papers*, vol. 69, no. 4, pp. 1788–1799, 2022.
- [7] R. Lu, R. Bai, R. Li, L. Zhu, M. Sun, F. Xiao, D. Wang, H. Wu, and Y. Ding, “A novel sequence-to-sequence-based deep learning model for multistep load forecasting,” *IEEE Transactions on Neural Networks and Learning Systems*, vol. 36, no. 1, pp. 638–652, 2025.
- [8] J. Lou, Y. Jiang, Q. Shen, R. Wang, and Z. Li, “Probabilistic regularized extreme learning for robust modeling of traffic flow forecasting,” *IEEE Transactions on Neural Networks and Learning Systems*, vol. 34, no. 4, pp. 1732–1741, 2023.
- [9] Z. Zhang, Y. Dong, and W.-C. Hong, “Long short-term memory-based twin support vector regression for probabilistic load forecasting,” *IEEE Transactions on Neural Networks and Learning Systems*, vol. 36, no. 1, pp. 1764–1778, 2025.
- [10] X. Wu, S. Mao, L. Xiong, and Y. Tang, “A survey on temporal network dynamics with incomplete data,” *Electronic Research Archive*, vol. 30, no. 10, pp. 3786–3810, 2022. [Online]. Available: <https://www.aimspress.com/article/doi/10.3934/era.2022193>
- [11] P. Ji, J. Ye, Y. Mu, W. Lin, Y. Tian, C. Hens, M. Perc, Y. Tang, J. Sun, and J. Kurths, “Signal propagation in complex networks,” *Physics reports*, vol. 1017, pp. 1–96, 2023.
- [12] Y. Tang, C. Zhao, J. Wang, C. Zhang, Q. Sun, W. X. Zheng, W. Du, F. Qian, and J. Kurths, “Perception and navigation in autonomous systems in the era of learning: A survey,” *IEEE Transactions on Neural Networks and Learning Systems*, vol. 34, no. 12, pp. 9604–9624, 2023.
- [13] A. Cini, I. Marisca, D. Zambon, and C. Alippi, “Graph deep learning for time series forecasting,” *arXiv preprint arXiv:2310.15978*, 2023.

[14] A. Cini, I. Marisca, F. M. Bianchi, and C. Alippi, "Scalable spatiotemporal graph neural networks," vol. 37, Jun. 2023, pp. 7218–7226. [Online]. Available: <https://ojs.aaai.org/index.php/AAAI/article/view/25880>

[15] Y. Tang, J. Kurths, W. Lin, E. Ott, and L. Kocarev, "Introduction to Focus Issue: When machine learning meets complex systems: Networks, chaos, and nonlinear dynamics," *Chaos: An Interdisciplinary Journal of Nonlinear Science*, vol. 30, no. 6, p. 063151, 06 2020. [Online]. Available: <https://doi.org/10.1063/5.0016505>

[16] H. Yu, T. Li, W. Yu, J. Li, Y. Huang, L. Wang, and A. Liu, "Regularized graph structure learning with semantic knowledge for multi-variate time-series forecasting," in *Proceedings of the Thirty-First International Joint Conference on Artificial Intelligence, IJCAI-22*, L. D. Raedt, Ed. International Joint Conferences on Artificial Intelligence Organization, 7 2022, pp. 2362–2368, main Track. [Online]. Available: <https://doi.org/10.24963/ijcai.2022/328>

[17] X. Zou, L. Xiong, Y. Tang, and J. Kurths, "Samsgl: Series-aligned multi-scale graph learning for spatiotemporal forecasting," *Chaos: An Interdisciplinary Journal of Nonlinear Science*, vol. 34, no. 6, p. 063140, 06 2024. [Online]. Available: <https://doi.org/10.1063/5.0211403>

[18] G. Ditzler, M. Roveri, C. Alippi, and R. Polikar, "Learning in non-stationary environments: A survey," *IEEE Computational Intelligence Magazine*, vol. 10, no. 4, pp. 12–25, 2015.

[19] N. Passalis, A. Tefas, J. Kanniaiainen, M. Gabbouj, and A. Iosifidis, "Deep adaptive input normalization for time series forecasting," *IEEE transactions on neural networks and learning systems*, vol. 31, no. 9, pp. 3760–3765, 2019.

[20] J. Ji, J. Wang, C. Huang, J. Wu, B. Xu, Z. Wu, J. Zhang, and Y. Zheng, "Spatio-temporal self-supervised learning for traffic flow prediction," in *Proceedings of the AAAI Conference on Artificial Intelligence*, vol. 37, no. 4, Jun. 2023, pp. 4356–4364. [Online]. Available: <https://ojs.aaai.org/index.php/AAAI/article/view/25555>

[21] Q. Tan, M. Ye, A. J. Ma, B. Yang, T. C.-F. Yip, G. L.-H. Wong, and P. C. Yuen, "Explainable uncertainty-aware convolutional recurrent neural network for irregular medical time series," *IEEE Transactions on Neural Networks and Learning Systems*, vol. 32, no. 10, pp. 4665–4679, 2021.

[22] T. Kim, J. Kim, Y. Tae, C. Park, J.-H. Choi, and J. Choo, "Reversible instance normalization for accurate time-series forecasting against distribution shift," in *International Conference on Learning Representations*, 2022. [Online]. Available: <https://openreview.net/forum?id=cGDAkQo1C0p>

[23] Y. Liu, H. Wu, J. Wang, and M. Long, "Non-stationary transformers: Exploring the stationarity in time series forecasting," in *Advances in Neural Information Processing Systems*, S. Koyejo, S. Mohamed, A. Agarwal, D. Belgrave, K. Cho, and A. Oh, Eds., vol. 35. Curran Associates, Inc., 2022, pp. 9881–9893. [Online]. Available: https://proceedings.neurips.cc/paper_files/paper/2022/file/4054556fcaa934b0bf76da52cf4f92cb-Paper-Conference.pdf

[24] K. Malialis, C. G. Panayiotou, and M. M. Polycarpou, "Online learning with adaptive rebalancing in nonstationary environments," *IEEE Transactions on Neural Networks and Learning Systems*, vol. 32, no. 10, pp. 4445–4459, 2021.

[25] W. Fan, P. Wang, D. Wang, Y. Zhou, and Y. Fu, "Dish-ts: A general paradigm for alleviating distribution shift in time series forecasting," in *Proceedings of the AAAI Conference on Artificial Intelligence*, vol. 37, no. 6, Jun. 2023, pp. 7522–7529. [Online]. Available: <https://ojs.aaai.org/index.php/AAAI/article/view/25914>

[26] L. Zhao, Y. Song, C. Zhang, Y. Liu, P. Wang, T. Lin, M. Deng, and H. Li, "Tgen: A temporal graph convolutional network for traffic prediction," *IEEE Transactions on Intelligent Transportation Systems*, vol. 21, no. 9, pp. 3848–3858, 2020.

[27] B. Yu, H. Yin, and Z. Zhu, "Spatio-temporal graph convolutional networks: A deep learning framework for traffic forecasting," in *Proceedings of the 27th International Joint Conference on Artificial Intelligence*, ser. IJCAI'18. AAAI Press, 2018, p. 3634–3640.

[28] Y. Seo, M. Defferrard, P. Vandergheynst, and X. Bresson, "Structured sequence modeling with graph convolutional recurrent networks," in *Neural Information Processing*, L. Cheng, A. C. S. Leung, and S. Ozawa, Eds. Cham: Springer International Publishing, 2018, pp. 362–373.

[29] S. Lan, Y. Ma, W. Huang, W. Wang, H. Yang, and P. Li, "Dstagnn: Dynamic spatial-temporal aware graph neural network for traffic flow forecasting," in *International conference on machine learning*. PMLR, 2022, pp. 11906–11917.

[30] H. Liu, Z. Dong, R. Jiang, J. Deng, J. Deng, Q. Chen, and X. Song, "Spatio-temporal adaptive embedding makes vanilla transformer sota for traffic forecasting," in *Proceedings of the 32nd ACM International Conference on Information and Knowledge Management*, ser. CIKM '23. New York, NY, USA: Association for Computing Machinery, 2023, p. 4125–4129. [Online]. Available: <https://doi.org/10.1145/3583780.3615160>

[31] F. Li, J. Feng, H. Yan, G. Jin, F. Yang, F. Sun, D. Jin, and Y. Li, "Dynamic graph convolutional recurrent network for traffic prediction: Benchmark and solution," *ACM Trans. Knowl. Discov. Data*, vol. 17, no. 1, feb 2023. [Online]. Available: <https://doi.org/10.1145/3532611>

[32] Y. Fang, K. Ren, C. Shan, Y. Shen, Y. Li, W. Zhang, Y. Yu, and D. Li, "Learning decomposed spatial relations for multi-variate time-series modeling," in *Proceedings of the AAAI Conference on Artificial Intelligence*, vol. 37, no. 6, Jun. 2023, pp. 7530–7538. [Online]. Available: <https://ojs.aaai.org/index.php/AAAI/article/view/25915>

[33] C. Xu and Y. Xie, "Conformal prediction interval for dynamic time-series," in *Proceedings of the 38th International Conference on Machine Learning*, ser. Proceedings of Machine Learning Research, M. Meila and T. Zhang, Eds., vol. 139. PMLR, 18–24 Jul 2021, pp. 11559–11569. [Online]. Available: <https://proceedings.mlr.press/v139/xu21h.html>

[34] S. H. Sun and R. Yu, "Copula conformal prediction for multi-step time series prediction," in *The Twelfth International Conference on Learning Representations*, 2024. [Online]. Available: <https://openreview.net/forum?id=ojIJZDNIBj>

[35] Y. Liang, Y. Xia, S. Ke, Y. Wang, Q. Wen, J. Zhang, Y. Zheng, and R. Zimmermann, "Airformer: Predicting nationwide air quality in china with transformers," in *Proceedings of the AAAI Conference on Artificial Intelligence*, vol. 37, no. 12, Jun. 2023, pp. 14329–14337. [Online]. Available: <https://ojs.aaai.org/index.php/AAAI/article/view/26676>

[36] J. Gan, R. Hu, Y. Mo, Z. Kang, L. Peng, Y. Zhu, and X. Zhu, "Multigraph fusion for dynamic graph convolutional network," *IEEE Transactions on Neural Networks and Learning Systems*, vol. 35, no. 1, pp. 196–207, 2024.

[37] C. Song, Y. Lin, S. Guo, and H. Wan, "Spatial-temporal synchronous graph convolutional networks: A new framework for spatial-temporal network data forecasting," vol. 34, Apr. 2020, pp. 914–921. [Online]. Available: <https://ojs.aaai.org/index.php/AAAI/article/view/5438>

[38] M. R. Taylor, K. C. Dhuyvetter, and T. L. Kastens, "Incorporating current information into historical-average-based forecasts to improve crop price basis forecasts," 2004.

[39] S. L. Ho and M. Xie, "The use of arima models for reliability forecasting and analysis," *Computers & industrial engineering*, vol. 35, no. 1-2, pp. 213–216, 1998.

[40] G. P. Zhang, "Time series forecasting using a hybrid arima and neural network model," *Neurocomputing*, vol. 50, pp. 159–175, 2003.

[41] T. Cheng and J. Wang, "Application of a dynamic recurrent neural network in spatio-temporal forecasting," in *Information Fusion and Geographic Information Systems: Proceedings of the Third International Workshop*. Springer, 2007, pp. 173–186.

[42] R. Fu, Z. Zhang, and L. Li, "Using lstm and gru neural network methods for traffic flow prediction," in *2016 31st Youth academic annual conference of Chinese association of automation (YAC)*. IEEE, 2016, pp. 324–328.

[43] H. Wu, T. Hu, Y. Liu, H. Zhou, J. Wang, and M. Long, "Timesnet: Temporal 2d-variation modeling for general time series analysis," in *The Eleventh International Conference on Learning Representations*, 2023. [Online]. Available: https://openreview.net/forum?id=ju_Uqw3840d

[44] S. He, J. Ji, and M. Lei, "Decomposed spatio-temporal mamba for long-term traffic prediction," in *Proceedings of the AAAI Conference on Artificial Intelligence*, vol. 39, no. 11, 2025, pp. 11772–11780.

[45] H. Zhou, S. Zhang, J. Peng, S. Zhang, J. Li, H. Xiong, and W. Zhang, "Informer: Beyond efficient transformer for long sequence time-series forecasting," vol. 35, no. 12, May 2021, pp. 11106–11115. [Online]. Available: <https://ojs.aaai.org/index.php/AAAI/article/view/17325>

[46] Y. Nie, N. H. Nguyen, P. Sinthong, and J. Kalagnanam, "A time series is worth 64 words: Long-term forecasting with transformers," in *The Eleventh International Conference on Learning Representations*, 2023. [Online]. Available: <https://openreview.net/forum?id=Jbdc0vTOcol>

[47] S. Wu, X. Xiao, Q. Ding, P. Zhao, Y. Wei, and J. Huang, "Adversarial sparse transformer for time series forecasting," in *Advances in Neural Information Processing Systems*, H. Larochelle, M. Ranzato, R. Hadsell, M. Balcan, and H. Lin, Eds., vol. 33. Curran Associates, Inc., 2020, pp. 17105–17115. [Online]. Available: https://proceedings.neurips.cc/paper_files/paper/2020/file/c6b8c8d762da15fa8dbdfb6baf9e260-Paper.pdf

[48] T. Zhou, Z. Ma, Q. Wen, X. Wang, L. Sun, and R. Jin, "FEDformer: Frequency enhanced decomposed transformer for long-term series forecasting," in *Proceedings of the 39th International Conference on Machine Learning*, ser. Proceedings of Machine Learning Research,

K. Chaudhuri, S. Jegelka, L. Song, C. Szepesvari, G. Niu, and S. Sabato, Eds., vol. 162. PMLR, 17–23 Jul 2022, pp. 27268–27286. [Online]. Available: <https://proceedings.mlr.press/v162/zhou22g.html>

[49] Y. Zhang and J. Yan, “Crossformer: transformer utilizing cross-dimension dependency for multivariate time series forecasting,” in *The Eleventh International Conference on Learning Representations*, 2023. [Online]. Available: <https://openreview.net/forum?id=vSVLm2j9eie>

[50] D. Song, S. Dai, W. Li, T. Ren, Z. Wei, and A.-A. Liu, “Stvformer: A spatial-temporal-variable transformer with auxiliary knowledge for sea surface temperature prediction,” *Applied Ocean Research*, vol. 153, p. 104218, 2024.

[51] H. Wu, H. Zhou, M. Long, and J. Wang, “Interpretable weather forecasting for worldwide stations with a unified deep model,” *Nature Machine Intelligence*, vol. 5, pp. 602–611, June 2023.

[52] H. Wu, J. Xu, J. Wang, and M. Long, “Autoformer: Decomposition transformers with auto-correlation for long-term series forecasting,” in *Advances in Neural Information Processing Systems*, M. Ranzato, A. Beygelzimer, Y. Dauphin, P. Liang, and J. W. Vaughan, Eds., vol. 34. Curran Associates, Inc., 2021, pp. 22419–22430. [Online]. Available: https://proceedings.neurips.cc/paper_files/paper/2021/file/bcc0d400288793e8bdc7c19a8ac0c2b-Paper.pdf

[53] B. N. Oreshkin, D. Carpol, N. Chapados, and Y. Bengio, “N-beats: Neural basis expansion analysis for interpretable time series forecasting,” in *International Conference on Learning Representations*, 2020. [Online]. Available: <https://openreview.net/forum?id=r1ecqn4YwB>

[54] C. Challu, K. G. Olivares, B. N. Oreshkin, F. Garza Ramírez, M. Mergenthaler Canseco, and A. Dubrawski, “Nhits: Neural hierarchical interpolation for time series forecasting,” vol. 37, pp. 6989–6997, Jun. 2023. [Online]. Available: <https://ojs.aaai.org/index.php/AAAI/article/view/25854>

[55] N. Rathore, P. Rathore, A. Basak, S. H. Nistala, and V. Runkana, “Multi scale graph wavenet for wind speed forecasting,” in *2021 IEEE International Conference on Big Data (Big Data)*. IEEE, 2021, pp. 4047–4053.

[56] J. Jiang, C. Han, W. X. Zhao, and J. Wang, “Pdformer: Propagation delay-aware dynamic long-range transformer for traffic flow prediction,” in *Proceedings of the AAAI Conference on Artificial Intelligence*, vol. 37, no. 4, Jun. 2023, pp. 4365–4373. [Online]. Available: <https://ojs.aaai.org/index.php/AAAI/article/view/25556>

[57] L. Bai, L. Yao, C. Li, X. Wang, and C. Wang, “Adaptive graph convolutional recurrent network for traffic forecasting,” in *Advances in Neural Information Processing Systems*, vol. 33. Curran Associates, Inc., 2020, pp. 17804–17815. [Online]. Available: https://proceedings.neurips.cc/paper_files/paper/2020/file/ce1aad92b939420fc17005e5461e6f48-Paper.pdf

[58] M. Ju, S. Hou, Y. Fan, J. Zhao, Y. Ye, and L. Zhao, “Adaptive kernel graph neural network,” in *Proceedings of the AAAI Conference on Artificial Intelligence*, vol. 36, no. 6, Jun. 2022, pp. 7051–7058. [Online]. Available: <https://ojs.aaai.org/index.php/AAAI/article/view/20664>

[59] W. Zheng and J. Hu, “Multivariate time series prediction based on temporal change information learning method,” *IEEE Transactions on Neural Networks and Learning Systems*, vol. 34, no. 10, pp. 7034–7048, 2023.

[60] Q. Liu, L. Long, H. Peng, J. Wang, Q. Yang, X. Song, A. Riscos-Núñez, and M. J. Pérez-Jiménez, “Gated spiking neural p systems for time series forecasting,” *IEEE Transactions on Neural Networks and Learning Systems*, vol. 34, no. 9, pp. 6227–6236, 2023.

[61] K. Zhang, X. Zou, and Y. Tang, “Caformer: Rethinking time series analysis from causal perspective,” *arXiv preprint arXiv:2403.08572*, 2024.

[62] R. Jiang, Z. Wang, J. Yong, P. Jeph, Q. Chen, Y. Kobayashi, X. Song, S. Fukushima, and T. Suzumura, “Spatio-temporal meta-graph learning for traffic forecasting,” in *Proceedings of the AAAI Conference on Artificial Intelligence*, vol. 37, no. 7, Jun. 2023, pp. 8078–8086. [Online]. Available: <https://ojs.aaai.org/index.php/AAAI/article/view/25976>

[63] R.-G. Cirstea, C. Guo, B. Yang, T. Kieu, X. Dong, and S. Pan, “Triformer: Triangular, variable-specific attentions for long sequence multivariate time series forecasting,” in *Proceedings of the Thirty-First International Joint Conference on Artificial Intelligence, IJCAI-22*, L. D. Raedt, Ed. International Joint Conferences on Artificial Intelligence Organization, 7 2022, pp. 1994–2001, main Track. [Online]. Available: <https://doi.org/10.24963/ijcai.2022/277>

[64] Q. Sun, J. Li, H. Peng, J. Wu, X. Fu, C. Ji, and P. S. Yu, “Graph structure learning with variational information bottleneck,” in *Proceedings of the AAAI Conference on Artificial Intelligence*, vol. 36, no. 4, Jun. 2022, pp. 4165–4174. [Online]. Available: <https://ojs.aaai.org/index.php/AAAI/article/view/20335>

[65] J. Deng, X. Chen, R. Jiang, X. Song, and I. W. Tsang, “St-norm: Spatial and temporal normalization for multi-variate time series forecasting,” in *Proceedings of the 27th ACM SIGKDD Conference on Knowledge Discovery & Data Mining*, ser. KDD ’21. New York, NY, USA: Association for Computing Machinery, 2021, p. 269–278. [Online]. Available: <https://doi.org/10.1145/3447548.3467330>

[66] X. Ma, X. Li, L. Fang, T. Zhao, and C. Zhang, “U-mixer: An unet-mixer architecture with stationarity correction for time series forecasting,” *arXiv preprint arXiv:2401.02236*, 2024.

[67] Z. Wang, R. Jiang, H. Xue, F. D. Salim, X. Song, R. Shibasaki, W. Hu, and S. Wang, “Learning spatio-temporal dynamics on mobility networks for adaptation to open-world events,” *Artificial Intelligence*, vol. 335, p. 104120, 2024. [Online]. Available: <https://www.sciencedirect.com/science/article/pii/S0004370224000560>

[68] B. W. Silverman, *Density estimation for statistics and data analysis*. Routledge, 2018.

[69] Y. Qin, D. Song, H. Cheng, W. Cheng, G. Jiang, and G. W. Cottrell, “A dual-stage attention-based recurrent neural network for time series prediction,” in *Proceedings of the 26th International Joint Conference on Artificial Intelligence*, ser. IJCAI’17. AAAI Press, 2017, p. 2627–2633.

[70] D. Luo, W. Cheng, Y. Wang, D. Xu, J. Ni, W. Yu, X. Zhang, Y. Liu, Y. Chen, H. Chen, and X. Zhang, “Time series contrastive learning with information-aware augmentations,” vol. 37, pp. 4534–4542, Jun. 2023. [Online]. Available: <https://ojs.aaai.org/index.php/AAAI/article/view/25575>

[71] X. Zheng, T. Wang, W. Cheng, A. Ma, H. Chen, M. Sha, and D. Luo, “Parametric augmentation for time series contrastive learning,” in *The Twelfth International Conference on Learning Representations*, 2024. [Online]. Available: <https://openreview.net/forum?id=EIPLdFy3vp>

[72] S. Guo, Y. Lin, N. Feng, C. Song, and H. Wan, “Attention based spatial-temporal graph convolutional networks for traffic flow forecasting,” in *Proceedings of the AAAI Conference on Artificial Intelligence*, vol. 33, no. 01, Jul. 2019, pp. 922–929. [Online]. Available: <https://ojs.aaai.org/index.php/AAAI/article/view/3881>

[73] Y. Li, R. Yu, C. Shahabi, and Y. Liu, “Diffusion convolutional recurrent neural network: Data-driven traffic forecasting,” in *International Conference on Learning Representations*, 2018. [Online]. Available: <https://openreview.net/forum?id=SJiHXGWAZ>

[74] R. Jiang, Z. Wang, J. Yong, P. Jeph, Q. Chen, Y. Kobayashi, X. Song, S. Fukushima, and T. Suzumura, “Spatio-temporal meta-graph learning for traffic forecasting,” in *Proceedings of the AAAI Conference on Artificial Intelligence*, vol. 37, no. 7, Jun. 2023, pp. 8078–8086. [Online]. Available: <https://ojs.aaai.org/index.php/AAAI/article/view/25976>

[75] H. Lee and S. Ko, “TESTAM: A time-enhanced spatio-temporal attention model with mixture of experts,” in *The Twelfth International Conference on Learning Representations*, 2024.

[76] Z. Cai, R. Jiang, X. Yang, Z. Wang, D. Guo, H. H. Kobayashi, X. Song, and R. Shibasaki, “Memda: Forecasting urban time series with memory-based drift adaptation,” ser. CIKM ’23. New York, NY, USA: Association for Computing Machinery, 2023, p. 193–202. [Online]. Available: <https://doi.org/10.1145/3583780.3614962>

[77] H. Hersbach, B. Bell, P. Berrisford, S. Hirahara, A. Horányi, J. Muñoz-Sabater, J. Nicolas, C. Peubey, R. Radu, D. Schepers, A. Simmons, C. Soci, S. Abdalla, X. Abellán, G. Balsamo, P. Bechtold, G. Biavati, J. Bidlot, M. Bonavita, G. De Chiara, P. Dahlgren, D. Dee, M. Diamantakis, R. Dragani, J. Flemming, R. Forbes, M. Fuentes, A. Geer, L. Haimberger, S. Healy, R. J. Hogan, E. Hólm, M. Janisková, S. Keeley, P. Laloyaux, P. Lopez, C. Lupu, G. Radnoti, P. de Rosnay, I. Rozum, F. Vamborg, S. Villaume, and J.-N. Thépaut, “The era5 global reanalysis,” *Quarterly Journal of the Royal Meteorological Society*, vol. 146, no. 730, pp. 1999–2049, 2020. [Online]. Available: <https://rmets.onlinelibrary.wiley.com/doi/abs/10.1002/qj.3803>

[78] C. Chen, K. Petty, A. Skabardonis, P. Varaiya, and Z. Jia, “Freeway performance measurement system: mining loop detector data,” *Transportation research record*, vol. 1748, no. 1, pp. 96–102, 2001.

[79] A. Vaswani, N. Shazeer, N. Parmar, J. Uszkoreit, L. Jones, A. N. Gomez, L. u. Kaiser, and I. Polosukhin, “Attention is all you need,” in *Advances in Neural Information Processing Systems*, I. Guyon, U. V. Luxburg, S. Bengio, H. Wallach, R. Fergus, S. Vishwanathan, and R. Garnett, Eds., vol. 30. Curran Associates, Inc., 2017. [Online]. Available: https://proceedings.neurips.cc/paper_files/paper/2017/file/3f5ee243547dee91fbd053c1c4a845aa-Paper.pdf